
SEMIPARAMETRIC POINT PROCESS MODELLING OF BLINKING ARTIFACTS IN PALM

PREPRINT

Louis G. Jensen* Department of Mathematics Aarhus University Aarhus C Denmark	David J. Williamson Randall Division for Cell and Molecular Biophysics King's College London London UK	Ute Hahn Department of Mathematics Aarhus University Aarhus C Denmark
--	---	--

July 17, 2022

ABSTRACT

Photoactivated localization microscopy (PALM) is a powerful imaging technique for characterization of protein organization in biological cells. Due to the stochastic blinking of fluorescent probes, and camera discretization effects, each protein gives rise to a cluster of artificial observations. These blinking artifacts are an obstacle for qualitative analysis of PALM data, and tools for their correction are in high demand. We develop the Independent Blinking Cluster point process (IBCpp) family of models, and present results on the mark correlation function. We then construct the PALM-IBCpp - a semiparametric IBCpp tailored for PALM data. We describe a procedure for estimation of parameters, which can be used without parametric assumptions on the spatial organization of proteins. The parameters include the kinetic rates that control blinking, and as such can be used to correct subsequent data analysis. The method is demonstrated on real data, and in a simulation study, where blinking artifacts were precisely quantified in a range of realistic settings.

Keywords Photoactivated localization microscopy · Multiple blinking · Spatio-temporal point patterns · Mark correlation function · Moment-based estimation · Second-order characteristics

1 Introduction

In their 2006 paper (Betzig et al. 2006), Eric Betzig and his collaborators showed how it is possible to localize multiple fluorescing proteins within a diffraction limited spot, using photoactiveable fluorescent proteins (PA-FP). PA-FPs can be activated, read, and permanently photobleached in stochastic fashion. By splitting up the fluorescent signal coming from different PA-FP into separate time intervals, each protein can be independently localized with high precision, even when they are closely located in space (Yamanaka et al. 2014).

Unfortunately, it is the nature of PA-FPs to stochastically enter and reemerge from dark states a number of times before permanently bleaching, leading to multiple appearances of the same protein (Annibale et al. 2011a, Fricke et al. 2015). For analysis of the spatial organization of molecules, these reappearances lead to erroneous conclusions, unless explicitly dealt with (Shivanandan et al. 2014). In addition, camera discretization effects complicate and exacerbate the multiple appearance problem (Griffié et al. 2020, Patel et al. 2019), and an understanding of both PA-FP photophysics and camera discretization effects is thus required to properly remedy the situation.

Although such artifacts are best understood by considering the spatio-temporal behavior of PA-FPs, little has been done to exploit both the spatial and temporal dimensions when analyzing blinking artifacts. In methods such as (Andersen et al. 2018, Sengupta et al. 2011), the spatial data alone is used, and require a model for protein behavior. Other methods use the temporal fluorescence traces to estimate the number of proteins in local regions (Hummer et al. 2016,

* Corresponding author

Email address: loga@math.au.dk

Karathanasis et al. 2017, Lin et al. 2015), which require either manual segmentation or external calibration samples. More recently, complex descriptions of PA-FP photophysics have been modeled by means of Hidden Markov Models (HMM) (Staudt et al. 2020, Patel et al. 2019). In (Patel et al. 2019), estimation is carried out by means of a calibration sample of well-separated fluorophores. In (Staudt et al. 2020), the authors model the conglomerate fluorescent intensity trace over a sequence of time points, as originating from some unknown number of PA-FP. This means that additional parameters have to be estimated, and the information in the spatial dimension is not exploited. Although these methods are powerful, and offer highly realistic modeling of the fluorescent probes, they rely on intricate numerical routines to optimize the (pseudo)-likelihood function, and are perhaps most relevant when the PA-FP themselves are of primary interest.

In this paper, we introduce a modeling and estimation framework for analyzing data from PALM microscopy, with a focus on quick estimation of blinking artifacts. The results and methods are built on a class of realistic, semiparametric cluster point processes for the observed spatio-temporal data, and estimation is carried out using moment methods. Our approach leads to estimates of the kinetic rates that govern photoblinking, which can be used to quantify the effect of blinking artifacts on a given sample. Blinking rates are estimated without a need for parametric modeling of the spatial organization of proteins, allowing the methods to be applied to essentially any PA-FP experiment.

The paper is organized as follows. In Section 2, we briefly go over the needed point process theory that will be used for modeling or estimation, and we give a quick rundown of the principles of PALM imaging, and how camera artifacts come into play. In Section 3, we define the family of Independent Blinking Cluster point processes, and present results on the mark correlation function. We then propose a particular model from the family, the PALM-IBCpp, for modeling of PALM data, and motivate the construction in terms of a discretized, 4-state PA-FP blinking model. In Section 4, we describe a procedure for estimation of the kinetic rates in the PA-FP blinking model. Section 5 considers a dataset expressing LAT-mEos3.2 PA-FP, and demonstrates the ability of the PALM-IBCpp to capture the spatio-temporal clustering behavior observed in real data. Finally, in Section 6, we simulate PA-FP with a range of different spatial organizations and blinking behaviors, and illustrate the ability of our estimation methods to precisely recover the blinking rates. We also include a misspecified blinking model, and show that important PA-FP descriptors, such as the total number of reappearances and time to bleaching, are still accurately recovered. Appendix A contains proofs of moment results hidden from the main text. Appendix B contains derivations of asymptotically exact, approximate expressions for discretized moment statistics needed for parameter estimation. In Appendix C we argue for the validity of using our estimation procedures, without modification, on samples with arbitrary protein organization. Finally, we propose a way of selecting informative query points for summary functions in Appendix D.

2 Prerequisites

In this section we present the notation and main point process concepts that we will be needing below, including moment measures, mark distributions, and the mark correlation function. We also explain some of the modeling difficulties that arise in super-resolution fluorescence microscopy experiments, namely those associated with discretization of the temporal information and background noise. For the general exposition, we work with processes on $\mathbb{R}^d \times \mathbb{R}_+$. For a more rigorous introduction to point process theory, we refer to (Daley & Vere-Jones 2007). For more on mark distributions, see (Stoyan 1984). Finally, more on the acquisition and preparation of super-resolution fluorescence microscopy data can be found in (Deschout et al. 2014).

2.1 Point processes and moment measures

For the purpose of this paper, a spatio-temporal point process, $V = \{(v_i, t_{v_i})\}_{i=1}^\infty$, is a random, locally finite point configuration with distinct points in $\mathbb{R}^d \times \mathbb{R}_+$. We assume the moment measures in the following are σ -finite.

Write $\downarrow V = \{v_i\}_{i=1}^\infty$ (*ground V*) for the random object obtained by stripping V of its times. Assume $\downarrow V$ is well-defined as a spatial point process on \mathbb{R}^d , having finite intensity function $\lambda_{\downarrow V}$ and second-order product density $\lambda_{\downarrow V}^{(2)}$. Then we compute the intensity measure, $\Lambda_{\downarrow V}$, and second-order factorial moment measure, $\alpha_{\downarrow V}^{(2)}$, as

$$\Lambda_{\downarrow V}(A) = \mathbb{E} \left[\sum_{v \in \downarrow V} \mathbb{1}_A(v) \right] = \int_A \lambda_{\downarrow V}(v) dv$$

$$\alpha_{\downarrow V}^{(2)}(A_1 \times A_2) = \mathbb{E} \left[\sum_{(v_1, v_2) \in \downarrow V}^{\neq} \mathbb{1}_{A_1 \times A_2}(v_1, v_2) \right] = \int_{A_1 \times A_2} \lambda_{\downarrow V}^{(2)}(v_1, v_2) d(v_1, v_2)$$

working everywhere on Borel sets, and we define the pair correlation function $g_{\downarrow V}$ in the usual way

$$g_{\downarrow V}(v_1, v_2) = \frac{\lambda_{\downarrow V}^{(2)}(v_1, v_2)}{\lambda_{\downarrow V}(v_1)\lambda_{\downarrow V}(v_2)}$$

We define the *1-point mark distribution*, $M_{V|v}^{(1)}$, as the conditional probability measure on \mathbb{R}_+ satisfying

$$\Lambda_V(A \times B) = \mathbb{E} \left[\sum_{(v, t_v) \in V} \mathbb{1}_A(v) \mathbb{1}_B(t_v) \right] = \int_A M_{V|v}^{(1)}(B) d\Lambda_V(v)$$

for arbitrary Borel sets A and B . Similarly, the *2-point mark distribution*, $M_{V|(v_1, v_2)}^{(2)}$, satisfies

$$\begin{aligned} \alpha_V^{(2)}(\times_{k=1}^2 [A_k \times B_k]) &= \mathbb{E} \left[\sum_{(v_1, t_{v_1}), (v_2, t_{v_2}) \in V}^{\neq} \mathbb{1}_{A_1 \times A_2}(v_1, v_2) \mathbb{1}_{B_1 \times B_2}(t_{v_1}, t_{v_2}) \right] \\ &= \int_{A_1 \times A_2} M_{V|(v_1, v_2)}^{(2)}(B_1 \times B_2) d\alpha_V^{(2)}(v_1, v_2) \end{aligned}$$

We then define the *mark correlation function*, k_V^f , as

$$k_V^f(v_1, v_2) = \frac{\int f(t_{v_1}, t_{v_2}) dM_{V|(v_1, v_2)}^{(2)}(t_{v_1}, t_{v_2})}{\int \int f(t_{v_1}, t_{v_2}) dM_{V|v_1}^{(1)}(t_{v_1}) dM_{V|v_2}^{(1)}(t_{v_2})} \quad (1)$$

for $f : \mathbb{R}_+^2 \mapsto \mathbb{R}_+$ a non-negative Borel function of two times. In the following, we will only need to work with mark distributions that are independent of the conditioning points, (v, v_1, v_2) , and we simply write $M_V^{(1)}$ and $M_V^{(2)}$.

2.2 PALM, discretization, and noise

To understand how PALM works, consider first a single fluorescent emitter located at the position x . Whenever fluorescence is emitted, it is captured by the camera, and the signal is integrated over the acquisition time lasting 1 frame. Based on the intensity profile observed on pixels, the position x is estimated, by assuming a shape for the point spread function (PSF) (Small & Stahlheber 2014, Ober et al. 2015), which models the blurry shape observed on a camera when imaging a point-source of light. The localization uncertainty associated with the estimate of x can then be computed, and is included in the dataset for each localization. This procedure was made possible because we assumed only a single, isolated fluorescent emitter. In a real biological sample, there can be several emitters at nearly the same position, and the assumption of an isolated signal is thus often violated. However, if we only receive a signal of finite length from each emitter, in non-overlapping windows of time, their spatial proximity becomes irrelevant, and we can again determine the position of each emitter. In PALM, this temporal separation is made possible using PA-FPs, which activate at different times, and turn off permanently after finite emission of fluorescence. In this way, at most a few emitters should be activate at a given space-time location, and they can then be individually localized.

Note that, using the procedure outlined above, each emitter will give rise to several localizations. To see why this is true, assume again that a single fluorescent emitter at position x sends out a (sufficiently bright) signal lasting in total T seconds, and the frame acquisition time is Δ seconds. We can then expect the signal to result in roughly $T\Delta^{-1}$ estimates of x , all of which will be included in the sample as separate localizations. Depending on the total fluorescence observed from the PA-FPs, and the camera framerate, this can lead to a large number of reappearances for each PA-FP. It is natural to think that this problem can be solved by grouping localization that are close in space-time, but this is a difficult problem in general. The localization uncertainty varies, and will occasionally take on large values. In addition, PA-FPs can enter temporary dark periods during which no fluorescence is emitted for a prolonged period of time. For these reasons, localizations arising from the same emitter can be relatively far removed from each other, and can thus be easily confused with those arising from a nearby, or even nonexistent, emitter. Further complicating such procedures is the lack of specific, *a priori* knowledge about the temporal behavior of the PA-FPs in the sample, making it hard to know how far in time it is reasonable to look for reappearances, or how many localizations to expect per grouping.

In addition to reappearances, background noise will invariably affect the dataset. Each time fluorescence is observed on the camera, it must be attributed as spurious background or coming from a PA-FP emission event, by means of a separating threshold. Since we cannot set the threshold too high without losing the signal of real PA-FP, some background noise points will always be present in PALM recordings.

3 Independent Blinking Cluster point processes

In this section we introduce the IBCpp family of models, which is a subset of clustered spatio-temporal point processes with a particular spatio-temporal clustering structure that is natural for modeling of super resolution microscopy data. We consider some moment results and summary statistics of interest for IBCpps, and finally construct the PALM-IBCpp, which is a semiparametric IBCpp model tailored for PALM data.

3.1 Definition

In specifying the IBCpp model, there are a few layers to cover. It is most natural to start by defining the spatio-temporal clusters, so let $C = (t_x, G, \{w_i\}_{i \in \mathbb{N}}, \{\epsilon_i\}_{i \in \mathbb{N}})$ be a collection of random objects associated with clustering. Here, t_x is a random variable on \mathbb{R}_+ referred to as the *activation time*, with marginal distribution denoted $M_X^{(1)}$. G is a finite random variable on \mathbb{N} , $\{w_i\}_{i \in \mathbb{N}}$ is a stochastic process on \mathbb{R}_+ , and $\{\epsilon_i\}_{i \in \mathbb{N}}$ is a collection of i.i.d. random variables on \mathbb{R}^d with radially symmetric, continuous density function h_ϵ . We allow for dependence between the variables in $(t_x, G, \{w_i\}_{i \in \mathbb{N}})$, but $\{\epsilon_i\}_{i \in \mathbb{N}}$ and $(t_x, G, \{w_i\}_{i \in \mathbb{N}})$ are assumed independent. Using these quantities, we define the *typical cluster* at $(x, t_x) \in \mathbb{R}^d \times \mathbb{R}_+$, by the expression

$$Y_{(x, t_x)} = \{y_i, t_{y_i}\}_{i=1}^G = \{x + \epsilon_i, t_x + w_i\}_{i=1}^G \quad (2)$$

Since we will need clusters at countably many locations, let $C_k = (t_{x_k}, G_k, \{w_{ki}\}_{i \in \mathbb{N}}, \{\epsilon_{ki}\}_{i \in \mathbb{N}})$ be defined such that the collection $\{C_k\}_{k \in \mathbb{N}}$ consists of i.i.d. collections, each having the same distribution as C .

Now, let $\downarrow X = \{x_i\}_{i=1}^\infty$ be a point process on \mathbb{R}^d . Using C_k , we mark each $x_k \in \downarrow X$ with the associate $t_{x_k} \in C_k$, so that

$$X = \{x_k, t_{x_k}\}_{k=1}^\infty \quad (3)$$

and we refer to X as the *protein process*. Similarly, using again C_k we define the *blinking cluster* at $(x_k, t_{x_k}) \in X$ via

$$Y_{(x_k, t_{x_k})} = \{x_k + \epsilon_{ki}, t_{x_k} + w_{ki}\}_{i=1}^{G_k} \quad (4)$$

By combining X with its clusters, we obtain the *blinking process* by

$$Z = \bigcup_{(x_k, t_{x_k}) \in X} Y_{(x_k, t_{x_k})} \quad (5)$$

Finally, let $E = \{e_i, t_{e_i}\}_{i=1}^\infty$ be a Poisson process (the *noise process*) independent of Z , with intensity function on the form

$$\lambda_E(e, t_e) = \lambda_{\downarrow E} \frac{\mathbb{1}(t_e \in [0, b])}{b} \quad (6)$$

for $0 < b < \infty$, $0 \leq \lambda_{\downarrow E} < \infty$. Then, we define the *Independent Blinking Cluster point process*, O , by the superposition

$$O = Z \bigcup E \quad (7)$$

As a remark on the definition, note that including t_{x_k} both in the clusters, and as the marks of X , is done primarily because it gives X the nice interpretation of being a process of origins, both in time and space, from which the clusters grow. It also explains our choice of notation for the distribution of t_x , $M_X^{(1)}$, which is then precisely the mark distribution of X .

3.2 Moment results

Throughout, let O be an IBCpp. Various simplifications of moment-based summary functions are available for O . Importantly, the mark correlation function takes a simple form. Although the estimation procedures of Section 4 can be used on general $\downarrow X$, the basis of these procedures is most clearly seen in the case where $\downarrow X$ is motion-invariant (stationary and rotation invariant) with well-defined intensity and pair correlation function, so we will assume that here, and refer to Appendix C for the general case. For clarity of exposition, we hide the derivations of the identities in this section - they can be seen in Appendix A.

Assume that G has finite first and second moments, and that f is a symmetric function of 2 arrival times. We also (trivially) assume that we are not only looking at noise, so that $\lambda_{\downarrow X} > 0$. Set

$$n_c = \frac{\mathbb{E}[G^2]}{\mathbb{E}[G]} - 1$$

$$\eta = \frac{\lambda_{\downarrow Z}}{\lambda_{\downarrow O}}$$

The intensity and pair correlation functions are then easily found

$$\lambda_{\downarrow Z} = \lambda_{\downarrow X} \mathbb{E}[G] \quad (8)$$

$$\lambda_{\downarrow O} = \lambda_{\downarrow Z} + \lambda_{\downarrow E} \quad (9)$$

$$g_{\downarrow O}(r) = \eta^2 (g_{\downarrow Z}(r) - 1) + 1 \quad (10)$$

$$g_{\downarrow Z}(r) = \frac{n_c}{\lambda_{\downarrow Z}} (h_\epsilon * h_\epsilon)(r) + (h_\epsilon * g_{\downarrow X})(r) \quad (11)$$

with

$$(h_\epsilon * h_\epsilon)(r) = \int h_\epsilon(o_1 - x) h_\epsilon(o_2 - x) dx$$

$$(h_\epsilon * g_{\downarrow X})(r) = \int \int g_{\downarrow X}(\|x_1 - x_2\|) h_\epsilon(o_1 - x_1) h_\epsilon(o_2 - x_2) dx_1 dx_2$$

for arbitrary (o_1, o_2) satisfying $\|o_1 - o_2\| = r$. For the mark correlation function, we consider first Z , for which we have

$$k_Z^f(r) g_{\downarrow Z}(r) = \frac{\gamma_1(f)}{\gamma_2(f)} \frac{n_c}{\lambda_{\downarrow Z}} (h_\epsilon * h_\epsilon)(r) + (h_\epsilon * g_{\downarrow X})(r) \quad (12)$$

where

$$\gamma_1(f) = \int \int f(t_1, t_2) dM_{Y_{(x_0, t_x)}}^{(2)}(t_1, t_2) dM_X^{(1)}(t_x) \quad (13)$$

$$\gamma_2(f) = \int \int f(t_1, t_2) dM_Z^{(1)}(t_1) dM_Z^{(1)}(t_2) \quad (14)$$

for arbitrary x_0 , and f such that $\gamma_2(f) > 0$. More explicitly, we have

$$\gamma_1(f) = \frac{\mathbb{E} \left[\sum_{(i,j)=1}^G \mathbb{1}(i \neq j) f(t_x + w_i, t_x + w_j) \right]}{\mathbb{E}[G(G-1)]} \quad (15)$$

$$\gamma_2(f) = \frac{\mathbb{E} \left[\sum_{i=1}^G \sum_{j=1}^{G'} f(t_x + w_i, t'_x + w'_j) \right]}{\mathbb{E}[G]^2} \quad (16)$$

where $(t'_x, G', \{w'_j\}_{j=1}^\infty)$ is an independent copy of the typical cluster quantity $(t_x, G, \{w_i\}_{i=1}^\infty)$. Similarly, for the observed IBCpp, \hat{O} , we have

$$k_{\hat{O}}^f(r) g_{\downarrow O}(r) = \eta^2 \frac{\gamma_2(f)}{\gamma_2^{\hat{O}}(f)} \left[k_Z^f(r) g_{\downarrow Z}(r) - 1 \right] + 1 \quad (17)$$

where

$$\gamma_2^{\hat{O}}(f) = \eta^2 \gamma_2(f) + (1 - \eta)^2 \gamma_2^E(f) + 2(1 - \eta) \eta \gamma_2^{EZ}(f)$$

$$\gamma_2^E(f) = \int \int f(t_1, t_2) dM_E^{(1)}(t_1) dM_E^{(1)}(t_2)$$

$$\gamma_2^{EZ}(f) = \int \int f(t_1, t_2) dM_E^{(1)}(t_1) dM_Z^{(1)}(t_2)$$

for f with $\gamma_2^{\hat{O}}(f) > 0$. Expanding the above, we see that

$$\gamma_2^{\hat{O}}(f) k_{\hat{O}}^f(r) g_{\downarrow O}(r) = \gamma_1(f) \left[\frac{\eta}{\lambda_{\downarrow O}} n_c (h_\epsilon * h_\epsilon)(r) \right] + \gamma_2(f) \left[\eta^2 ((h_\epsilon * g_{\downarrow X})(r) - 1) \right] + \gamma_2^{\hat{O}}(f) \quad (18)$$

And we have the important alternative characterization

$$\gamma_2^O(f)k_O^f(r)g_O(r) = (\gamma_1(f) - \gamma_2(f)) \left[\frac{\eta}{\lambda_O} n_c(h_\epsilon * h_\epsilon)(r) \right] + \gamma_2(f) [g_O(r) - 1] + \gamma_2^O(f) \quad (19)$$

obtained by simply combining (18) with (10) and (11). In (19), the influence of the protein locations, $\downarrow X$, is entirely contained in g_O , which can be estimated nonparametrically. This will allow us to estimate the kinetic blinking rates without specifying a model for the proteins in Section 4.

3.3 An IBCpp model for PALM data

In order to use the IBCpp family in practice, we get more specific about the construction of the typical cluster, and the noise process. The choices we make here are based on realistic models for fluorophore photophysics, camera discretization effects, and localization errors, and lead to the PALM-IBCpp model. In the following, we will assume that the spatial dimension is $d = 2$ everywhere. Of course, our methods can still be used for 3D-PALM recordings by simply discarding the z -coordinates before estimation. The reason we do not directly model 3D data is that the localization uncertainty is generally asymmetrical in the z dimension (Shtengel et al. 2009), and a radially symmetric noise profile is then no longer a valid assumption.

Dealing first with the spatial components, we need to specify the localization error density, h_ϵ . On the camera, a point source of light appears as a blurry spot, the shape of which is described by the PSF. We model the PSF associated with each localization using a symmetric Gaussian density function with variance ξ^2 . As ξ depends on the number of photons detected, and various other stochastic nuisance factors that can vary over time and space, it makes sense to treat ξ as random. As a simple approximation, we assume that ξ is drawn i.i.d. for each observation. Thus, denoting by $N(0, \xi^2)$ the density of the centered, symmetric Gaussian distribution in \mathbb{R}^2 with variance ξ^2 , we set

$$h_\epsilon(x) = \mathbb{E}[N(0, \xi^2)(x)] \quad (20)$$

where the mean is taken with respect to ξ . The use of Gaussian approximate PSFs is standard practice, and generally provides highly accurate results (Zhang et al. 2007).

Moving on to G and the temporal behavior of clusters, we take as basis a well-established 4-state model for continuous time fluorophore behavior (Griffié et al. 2020, Rollins et al. 2015, Coltharp et al. 2012). We imagine the PA-FP are independently following a Markov processes, with a single fluorescent state (F), and 3 non-fluorescent states, see Figure 1. The processes always begins in the inactive state (I), and eventually moves to the (F) state. From here, it can either go dark (D) temporarily, or permanently photobleach (B).

Unfortunately, we cannot observe the process in continuous time. To describe the fluorescent signal that is ultimately observed from a PA-FP during the experiment, write Δ for the length of 1 camera frame, and

$$e(t) = \begin{cases} 1 & \text{if the PA-FP is in state } F \text{ at time } t \\ 0 & \text{otherwise} \end{cases}$$

If no fluorescence was missed, we would then observe the discretized signal on camera frame k precisely when $e(t) = 1$ for any duration on frame k . In practice, there is a non-zero threshold on the amount of signal that must be observed during a given integration length period, but this threshold is generally set low when recording PALM images in practice (Patel et al. 2019), so we ignore it and simply model the activity on frame k with the idealized expression

$$\tilde{e}(k) = \mathbb{1}_{(0, \Delta]} \left(\int_{\Delta(k-1)}^{\Delta k} e(t) dt \right)$$

and the observed timepoints are then $k\Delta$ for k with $\tilde{e}(k) = 1$. Thinking of t_x as the temporal origin of a cluster, we therefore specify the cluster quantities $(t_x, G, \{w_i\}_{i=1}^\infty)$ as

$$G = \sum_{k=1}^{\infty} \tilde{e}(k) \quad (21)$$

$$t_x = \Delta \min\{s : \sum_{k=1}^s \tilde{e}(k) = 1\} \quad (22)$$

$$w_i = \begin{cases} \Delta \min\{s : \sum_{k=1}^s \tilde{e}(k) = i\} - t_x & \text{if } 1 \leq i \leq G \\ \infty & \text{otherwise} \end{cases} \quad (23)$$

where t_x , w_i , and G are understood to be computed from the same trace, $e(t)$, i.e. they are dependent. In this way, the timepoints of a typical cluster correspond precisely to the discretized signal in $\tilde{e}(k)$, see Figure 2. Finally, for the noise process, we simply need to specify b as the time at which the PALM recording was terminated.

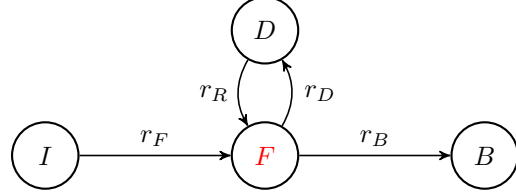


Figure 1: The transition diagram for the continuous time, photophysical model of fluorophores. Transitions are Markovian, with rates indicated next to the relevant transition arrows.

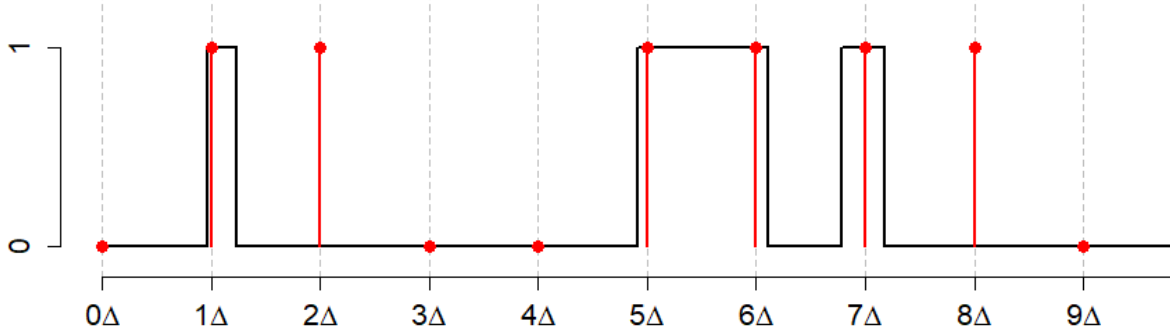


Figure 2: Camera discretization transforms the continuous process $e(t)$ (in black) into the discrete process $\tilde{e}(k)$ (in red). The observed timepoints are $k\Delta$ for k with $\tilde{e}(k) = 1$; in this example there are 6 such k , observed on frames $\{1, 2, 5, 6, 7, 8\}$, and we thus have $G = 6$, $t_x = \Delta$, $\{w_i\}_{i=1}^{\infty} = (0, \Delta, 4\Delta, 5\Delta, 6\Delta, 7\Delta, \infty, \infty, \dots)$.

4 Estimation

In the following, let $O = \{o_i, t_{o_i}\}_{i \in \mathbb{N}}$ be a PALM-IBCpp model, observed with N points in the window $W \times [0, b] \subset \mathbb{R}^2 \times \mathbb{R}_+$. There are several ways in which estimation of parameters of O could proceed. Here, we suggest an approach that estimates the cluster term auto-convolution, $(h_{\epsilon} * h_{\epsilon})$, and the 'signal fraction', η , before the kinetic rates. We will use approximate expressions for the theoretical moment quantities used in this section. The approximations are based on simplified discretization assumptions, and are asymptotically exact as $\Delta \rightarrow 0$; we refer to Appendix B for details. For clarity of exposition, we describe our methods here on the assumption that $\downarrow X$ be motion-invariant, but we point out again that the same methods can be used on general $\downarrow X$ without modification.

4.1 Summary statistics

We will be using moment methods, based on second-order statistics of the location and time behavior of the process. We write

$$d(t_1, t_2) = t_1 + t_2$$

$$P_u(t_1, t_2) = \mathbb{1}(|t_1 - t_2| \leq u)$$

and we set

$$S_O^f(r) = \gamma_2^O(f) k_O^f(r) g_O(r) \quad (24)$$

where we may estimate $\gamma_2^O(f) k_O^f$ as the (unnormalized) mark correlation function of O , and g_O is estimated also from O . Both quantities can be obtained using standard kernel estimators - for this work, we have used the implementations in the R package Spatstat (Baddeley et al. 2015). Combining two such estimators we get an estimate for S_O^f , which we will denote \hat{S}_O^f . In the following, we will work with S_O^f for $f = P_u$ for various u , and we assume that we have the estimate $\hat{S}_O^f(r)$ for r in a set $R = \{r_1, \dots, r_m\}$. Standard kernel estimator implementations have reasonable defaults for the set of r -values, but we describe a rule for selecting a set that is more appropriate for our needs in Appendix D.

4.2 Cluster autoconvolution

Localization software outputs an uncertainty for each localized emitter, and we will use this output to find the cluster autoconvolution, $(\widehat{h_\epsilon * h_\epsilon})(r)$. Recall that a PA-FP at location $x \in \mathbb{R}^2$ is observed with noise, so that the observed localization is instead given by $x + \epsilon$, where the distribution of ϵ does not depend on x or any other observation in the sample. Given the definition of h_ϵ in (20), we condition on (ξ_1, ξ_2) to obtain

$$(h_\epsilon * h_\epsilon)(r) = \int h_\epsilon(o_1 - x)h_\epsilon(o_2 - x)dx = \mathbb{E} \left[\frac{e^{-\frac{r^2}{2(\xi_1^2 + \xi_2^2)}}}{2\pi(\xi_1^2 + \xi_2^2)} \right]$$

for $\|o_1 - o_2\| = r$. Since our dataset includes an estimate of the localization uncertainty for each x_i , we estimate the autoconvolution by

$$(\widehat{h_\epsilon * h_\epsilon})(r) = \mathbb{E} \left[\frac{e^{-\frac{r^2}{2(\hat{\xi}_1^2 + \hat{\xi}_2^2)}}}{2\pi(\hat{\xi}_1^2 + \hat{\xi}_2^2)} \right] \quad (25)$$

where $\hat{\xi}_1$ and $\hat{\xi}_2$ are drawn from the observed distribution of localization uncertainties.

4.3 Background noise

Although there are generally only a small fraction of background noise points in a given region of interest (ROI), the way standard PALM imaging is conducted allows us to obtain a better estimate than the optimistic $\hat{\eta} = 1$. Typically, a part of bare imaging coverslip will be included in such a PALM recording, both because it adds a reference for the location of the ROI, and because the imaging window may be larger than the cell being imaged, see Figure 3. We assume that the only fluorescent signal coming from the bare part of the coverslip is attributed to background noise, and that the intensity of the noise process is constant across the imaging window.

Let $\downarrow O_{noise}$ be the noise process locations observed in a bare part of the coverslip. Under the assumptions above, we then have that O_{noise} is a stationary Poisson process with intensity $\lambda_{\downarrow E}$. Write W_{noise} for the region in which O_{noise} is observed. The standard estimator of $\lambda_{\downarrow E}$ is then

$$\hat{\lambda}_{\downarrow E} = \frac{|(O_{noise} \cap W_{noise})|}{|W_{noise}|}$$

where $|(O_{noise} \cap W_{noise})|$ denotes the number of points O_{noise} has in W_{noise} , and $|W_{noise}|$ is the area of W_{noise} . Using this estimator of $\lambda_{\downarrow E}$, we obtain

$$\hat{\eta} = 1 - \frac{\hat{\lambda}_{\downarrow E}}{\hat{\lambda}_{\downarrow O}} \quad (26)$$

where $\hat{\lambda}_{\downarrow O}$ is the estimated intensity of O .

4.4 Kinetic blinking rates

As a basis for estimation of blinking rates, $\hat{S}_O^{P_u}$ is first computed for u in $U \subset \mathbb{R}_+$. A good choice for the set U is discussed in Appendix D. We will also need an estimate of $\gamma_2^O(P_u)$ - the standard estimator is obtained by setting

$$\hat{\gamma}_2^O(P_u) = \frac{1}{N(N-1)} \sum_{i,j}^{\neq} P_u(t_{o_i}, t_{o_j})$$

where the sum is over all distinct pairs of timepoints in the observation window (Gelfand et al. 2010, p. 393).

In addition, we will need $\hat{\gamma}_2(P_u)$. From (14) we see that $\gamma_2(f)$ is simply the mean of f under 2 arrival times independently following the 1-point mark distribution of Z , $M_Z^{(1)}$. Thus, by estimating $M_Z^{(1)}$, it is trivial to obtain $\gamma_2(f)$ for any f . To do this, write $M_Z^{(1)}(u) = \int_0^u dM_Z^{(1)}(x)$ for the CDF associated with $M_Z^{(1)}$, and $M_O^{(1)}(u)$ similarly the CDF associated with the 1-point mark distribution of O , $M_O^{(1)}$. Then, it is easy to show that (see Appendix A)

$$M_O^{(1)}(u) = \eta M_Z^{(1)}(u) + (1 - \eta) \frac{u}{b}$$

Using $\hat{\eta}$ and replacing $M_O^{(1)}(u)$ with the observed arrival time CDF, we obtain

$$\hat{M}_Z^{(1)}(u) = \frac{N^{-1} \sum_{i=1}^N \mathbb{1}(t_{o_i} \leq u) - (1 - \hat{\eta}) \frac{u}{b}}{\hat{\eta}} \quad (27)$$

from which $\hat{\gamma}_2(P_u)$ is obtained numerically or by sampling. Now, write

$$\zeta_u = (\gamma_1(P_u) - \hat{\gamma}_2(P_u))n_c$$

and, solving a minimum contrast problem cf. the theoretical form of $S_O^{P_u}$ in (19) with estimated quantities in place of theoretical, we define the estimator

$$\hat{\zeta}_u = \frac{\hat{\lambda}_O}{\hat{\eta}} \frac{\sum_{r \in R} [\hat{S}_O^{P_u}(r) - \hat{\gamma}_2(P_u)(\hat{g}_O(r) - 1) - \hat{\gamma}_2^O(P_u)] \widehat{[(h_\epsilon * h_\epsilon)(r)]}}{\sum_{r \in R} \widehat{[(h_\epsilon * h_\epsilon)(r)]}^2} \quad (28)$$

for $u \in U$.

Using $\hat{\zeta}_u$, we set up the following minimization problem for 3 of the rates in the 4-state model:

$$\min_{r_D, r_R, r_B} \sum_{u \in U} (\hat{\zeta}_u - (\gamma_1(P_u) - \hat{\gamma}_2(P_u))n_c)^2 \quad (29)$$

where the rates control the values of $\gamma_1(P_u)$ and n_c . As we will see below, r_F has no impact on the minimization problem, and therefore does not appear. To optimize over the rates, we need expressions for $\gamma_1(P_u)$ and n_c . Closed-form expressions are not available due to complicated discretization effects, and simulation is generally too prohibitive to be used as part of an optimization regime. For these reasons, we will employ various approximations, we again refer to Appendix B for their derivations.

Define the following quantities, associated with the behavior of a PA-FP following the 4-state model

$$\begin{aligned} p &= \frac{r_B}{r_D + r_B} \\ N_b &\sim \text{Geom}_1(p) \\ W_F &\sim \text{Exp}(r_D + r_B) \\ W_D &\sim \text{Exp}(r_R) \\ W_I &\sim \text{Exp}(r_F) \\ \phi_R(v) &= \mathbb{E}[e^{ivW_R}] \\ \phi_F(v) &= \mathbb{E}[e^{ivW_F}] \\ \phi_{(F+R)}(v) &= \mathbb{E}[e^{ivW_F}] \mathbb{E}[e^{ivW_R}] \end{aligned}$$

where by Geom_1 we mean a geometric distribution starting from 1. Then, recall again that Δ is the frame integration length, and denote

$$\begin{aligned} A(v) &= \frac{2\mathbb{E}[N_b] \left(\phi_F(v)e^{-iv\Delta\frac{1}{2}} + \left(\frac{\mathbb{E}[W_F]}{\Delta} - \frac{1}{2} \right) (e^{-\Delta iv} - 1) - 1 \right)}{(1 - e^{-\Delta iv})^2} \\ B(v) &= \phi_R(v) (\mathbb{E}[\phi_{(F+R)}(v)^{N_b}] - 1 - \mathbb{E}[N_b](\phi_{(F+R)}(v) - 1)) \\ C(v) &= \frac{2e^{-iv\Delta 2}}{(1 - e^{-\Delta iv})^2} \left(\frac{\phi_F(v)e^{iv\Delta\frac{1}{2}} - 1}{\phi_{(F+R)}(v) - 1} \right)^2 \\ D &= \mathbb{E}[N_b^2] \left(\frac{\mathbb{E}[W_F]}{\Delta} + \frac{1}{2} \right)^2 + \mathbb{E}[N_b] \left[\frac{\mathbb{E}[W_F^2] - \mathbb{E}[W_F]^2}{\Delta^2} - \frac{\mathbb{E}[W_F]}{\Delta} - \frac{1}{2} \right] \end{aligned}$$

and the CDF $u \mapsto \gamma_1(P_u)$ then has associated characteristic function given as approximately

$$\phi(v) \approx \frac{A(v) + B(v)C(v)}{D} \quad (30)$$

and we can obtain $\gamma_1(P_u)$ by an inversion of $\phi(v)$. Since the approximations are based on continuous random variables, we use the simple numerical inversion scheme of (Davies 1973) for continuous distributions.

For n_c , we base our expression on an approximate distribution for G . We have

$$\begin{aligned}\mathbb{E}[G] &\approx \mathbb{E}[N_b] \left(\frac{\mathbb{E}[W_F]}{\Delta} + 1 \right) - \mathbb{E}[N_b - 1] \mu_R^1 \\ \mathbb{E}[G^2] &\approx \mathbb{E}[N_b^2] \left(\frac{\mathbb{E}[W_F]}{\Delta} + 1 \right)^2 + \mathbb{E}[N_b] \frac{\mathbb{E}[W_F^2] - \mathbb{E}[W_F]^2}{\Delta^2} \\ &\quad + \mathbb{E}[(N_b - 1)^2] (\mu_R^1)^2 + \mathbb{E}[N_b - 1] (\mu_R^2 - (\mu_R^1)^2) \\ &\quad - 2\mathbb{E}[N_b(N_b - 1)] \left(\frac{\mathbb{E}[W_F]}{\Delta} + 1 \right) \mu_R^1\end{aligned}$$

with

$$\begin{aligned}\mu_R^1 &= \int_0^1 (1-x) dP_{\frac{W_R}{\Delta}}(x) \\ \mu_R^2 &= \int_0^1 (1-x)^2 dP_{\frac{W_R}{\Delta}}(x)\end{aligned}$$

where $P_{\frac{W_R}{\Delta}}$ denotes the distribution of the scaled random variable $\frac{W_R}{\Delta}$. Now, since

$$n_c = \frac{\mathbb{E}[G^2]}{\mathbb{E}[G]} - 1$$

we obtain \hat{n}_c by substituting in the moments.

Minimizing (29) is done numerically, and results in estimates of (r_D, r_R, r_B) . The minimization problem is well-behaved and requires little supervision, but upper bounds can be utilized to speed up the process, and to avoid the exploration of extreme kinetic rates for which the approximations above can break down. Since r_F cannot be estimated in this way, we consider the relation

$$\mathbb{E}[W_I] \approx \frac{1}{2} \gamma_2(d) - A_2 - B_2$$

where

$$\begin{aligned}A_2 &= \frac{\frac{\mathbb{E}[W_F^2]}{2\Delta} + \mathbb{E}[W_F] + \frac{3\Delta}{8}}{\frac{\mathbb{E}[W_F]}{\Delta} + \frac{1}{2}} \\ B_2 &= \frac{\left(\frac{\mathbb{E}[W_F]}{\Delta} + \frac{1}{2} \right) \left(\frac{1}{2} \mathbb{E}[N_b(N_b - 1)] (\mathbb{E}[W_F] + \mathbb{E}[W_R]) + \mathbb{E}[N_b] \Delta \frac{1}{2} \right)}{\mathbb{E}[N_b] \left(\frac{\mathbb{E}[W_F]}{\Delta} + \frac{1}{2} \right)}\end{aligned}$$

Write \hat{A}_2 and \hat{B}_2 for the quantities A_2 and B_2 computed using the estimated $(\hat{r}_D, \hat{r}_R, \hat{r}_B)$. Finally, by estimating $\gamma_2(d)$ directly from the observed timepoints and $\hat{\eta}$, we obtain an estimator for r_F as

$$\hat{r}_F = \left(\frac{\frac{1}{N} \sum_{i=1}^N t_{o_i} - (1 - \hat{\eta}) \frac{b}{2}}{\hat{\eta}} - \hat{A}_2 - \hat{B}_2 \right)^{-1} \quad (31)$$

So far, we have silently assumed that all PA-FP have been imaged by the end of the experiment, that is, within the time window $[0, b]$. In practice, a recording is often allowed to run for a predetermined period of time, say 30-60 minutes, so this assumption is rarely true. Barring edge effects, this changes nothing about the way estimation should be carried out, or the validity of the estimated (η, r_D, r_R, r_B) and derived quantities, but the interpretation of \hat{r}_F as the rate of $W_I \sim \text{Exp}(r_F)$ no longer holds. Rather, \hat{r}_F^{-1} is then estimating the mean of the conditional distribution $(W_I | W_I < b)$. A corrected estimate can be found by numerically equating this mean with its theoretical counterpart, i.e. solving

$$\frac{e^{r_F^c b} - r_F^c b - 1}{r_F^c (e^{r_F^c b} - 1)} - \hat{r}_F^{-1} = 0$$

in r_F^c . Among other things, this corrected estimate can be used to estimate the total number of proteins that would have been imaged in the ROI W , had the experiment been allowed to run to completion. If \hat{r}_F^c is the corrected estimate and

$$N^b = \frac{\hat{\eta} \hat{\lambda}_{\text{O}} |W|}{\widehat{\mathbb{E}[G]}}$$

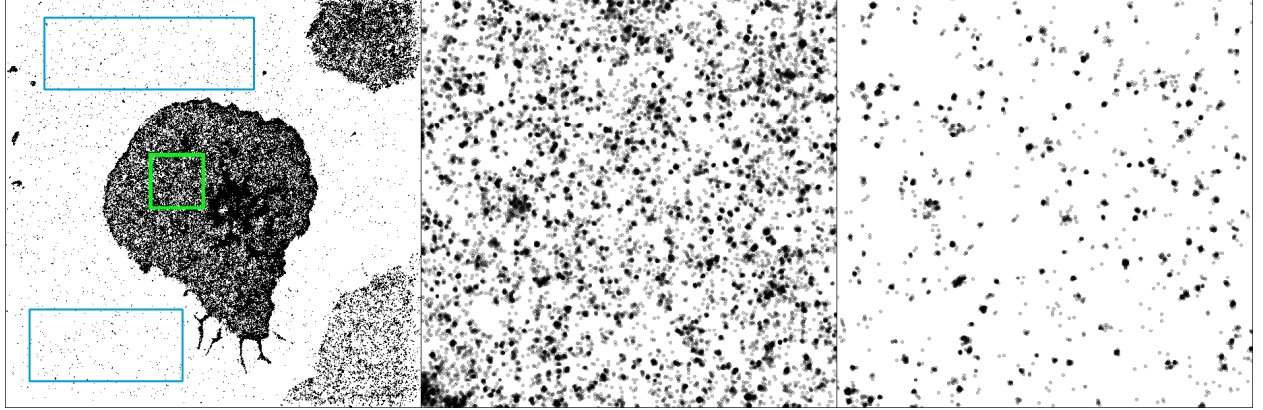


Figure 3: The full dataset (left) with green region of interest magnified (center). The blue regions were used for estimating the intensity of the noise process. After discarding the first 300 seconds of the recording, a reduced dataset is obtained (right).

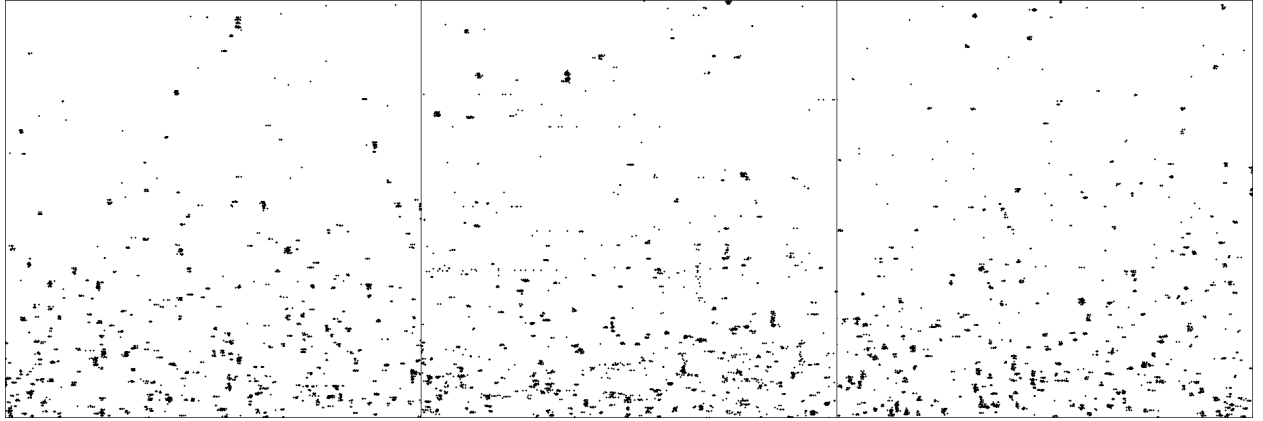


Figure 4: The observed data (center) with simulations from the fitted PALM-IBCpp on the left and right. The arrival times are plotted against the x-axis, illustrating the spatio-temporal clustering behavior.

is the estimated number of proteins imaged in W during the time interval $[0, b]$, we get the estimated total number of proteins in W (hidden and observed) as

$$N^\infty = \frac{N^b}{1 - e^{-\hat{r}_F^c b}} \quad (32)$$

5 Application to LAT-mEos3.2 data

We consider data from a 2D-PALM experiment. The sample is a Jurkat T cell which has been activated by, and form synapses against, antibody coated glass. It is expressing LAT-mEos3.2, and was imaged by TIRFM. The dataset was recorded at a framerate of $\Delta^{-1} = 25\text{hz}$, and was then resolved and corrected for drift using ThunderSTORM (Ovesný et al. 2014). Finally, the frame numbers were divided by the framerate, so that the arrival times are measured in seconds.

For analysis we first subset out a region of interest of manageable size. We further subset out 2 large regions from the coverslip outside the cell, which were used for estimation of η , see Figure 3. In addition, since the localization errors were slightly larger in the beginning of the experiment, we removed the first 300 seconds of the recording, at which time the errors had stabilized. The resulting sample had 3924 localizations in the ROI, and 1097 localizations in the (combined) noise region. After removing the first 300 seconds, all timepoints had 300 seconds subtracted, so that the new sample begins at time 0, and r_F can be correctly estimated. Note that the relative amount of background noise points will be higher in the later parts of the experiment, where most PA-FPs have activated and bleached. In our case,

we have $\hat{\eta} = 0.980$ for the subset data, whereas for the entire ROI we obtain $\hat{\eta} = 0.995$. This difference is important, and the latter estimate should be used if subsequent analysis is carried out on the entire ROI.

We fit the PALM-IBCpp model to the reduced sample, the results of which can be seen in Table 1, where we also include various important descriptors related to the blinking behavior, and results from a simulation refitting study. Simulations from the fitted model can be seen in Figure 4. The estimated parameters indicate that most of the clustering in this ROI can be explained by blinking clusters, so in simulations we have chosen a homogeneous Poisson process for X , conditioned on there being

$$|X| = \frac{3924 \cdot 0.98}{\mathbb{E}[G]} \approx 323$$

real, underlying proteins. The localization uncertainties were drawn i.i.d. from the observed uncertainties.

	Est	Avg	Sd
η	0.980	0.980	0.001
$r_F \cdot 10^3$	3.749	3.750	0.247
r_B	3.156	3.237	0.256
r_D	6.307	6.909	0.881
r_R	0.703	0.752	0.112
$\mathbb{E}[G]$	10.893	10.879	0.722
p	0.333	0.321	0.026
$q_{0.25}$	0.141	0.148	0.016
$q_{0.50}$	1.500	1.569	0.222
$q_{0.75}$	4.616	4.658	0.578
$q_{0.99}$	19.139	18.920	2.096

Table 1: Estimates (Est) obtained from the fit to the observed data. Included is average (Avg) and standard deviation (Sd) of estimates obtained from fitting to 100 simulations from the fitted model. Included derived quantities are: the mean number of reappearances, $\mathbb{E}[G]$, the bleaching probability, p , and the (0.25, 0.50, 0.75, 0.99)-quantiles ($q_{0.25}, q_{0.50}, q_{0.75}, q_{0.99}$) of the total PA-FP lifetime distribution (time in seconds from activation to bleaching).

6 Simulation study

We evaluate the performance of our estimation methods under different protein distributions and kinetic blinking rates. We will also consider what happens when the blinking model is misspecified. We consider 3 different cases of protein distributions: complete spatial randomness (CSR), spherical clustering, and fibrous structures, see Figure 5. We fix the number of proteins at $|X| = 500$ for all simulations, with localization uncertainties drawn i.i.d. from the $\text{Gamma}(6.5, 0.375)$ distribution (shape and rate parameterization), which is the maximum likelihood fit to the observed uncertainties in the real data example of Section 5, and we consider $\eta = 1$ known. For the fibers, $\downarrow X$ is neither stationary nor rotation invariant.

For the kinetic rates, we consider short and long lived PA-FP. Additionally, in a misspecified case, we use a model with 3 distinct dark states, each selected with the same probability, but with very different holding time distributions. For the values of the kinetic rates in the 3 PA-FP models, see Figure 6. We simulated 100 realizations from each combination of spatial organization and blinking behavior, and discretized signals according to a framerate of 25hz.

The results of the simulation study can be seen in Table 2. For the short and long lived PA-FP, we see that there is close correspondence between the true parameter values and their estimates, especially for the smaller rates and all derived blinking statistics. The mean number of reappearances is well estimated, as is the bleaching probability, p , and the total lifetime quantiles. Some bias appears to exist for the dark-state return rate, r_D , which also has the highest uncertainty of the rates. This is likely due to the bias in the utilized approximations for low framerate to rate ratios. Importantly, for the misspecified 3 dark-states model, the number of reappearances and the lifetime quantiles are again well estimated. Unsurprisingly, both r_B and p are biased in this case, as the model attempts to fit to an average blinking cycle, and cannot exactly capture the nuances of having 3 different dark states. Overall, the effect of the protein distribution is small compared to the effect of different PA-FP models, with a slight increase in variance for more clustered conditions.

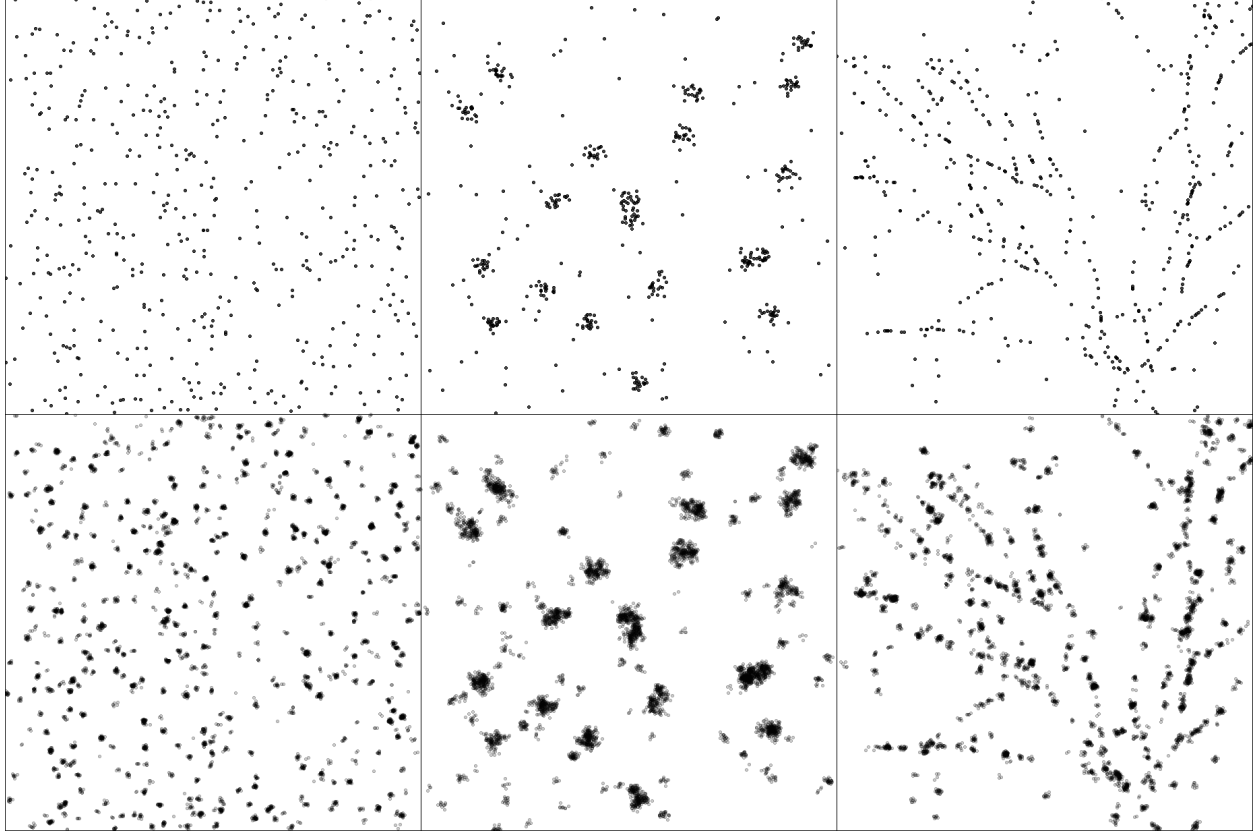


Figure 5: Typical simulations from each of the 3 protein configurations (CSR, clusters, fibers) in the columns, before and after adding blinking clusters in the top and bottom rows, respectively. The CSR data is simulated as 500 i.i.d. uniform points in the ROI. The clusters data consists of 100 CSR points and further 20 uniformly located Gaussian clusters with standard deviation 50, each having 20 points. Finally, for the fiber data, 450 points are sampled uniformly along the edges of a fixed fiber structure, and 50 CSR points are added to the background.

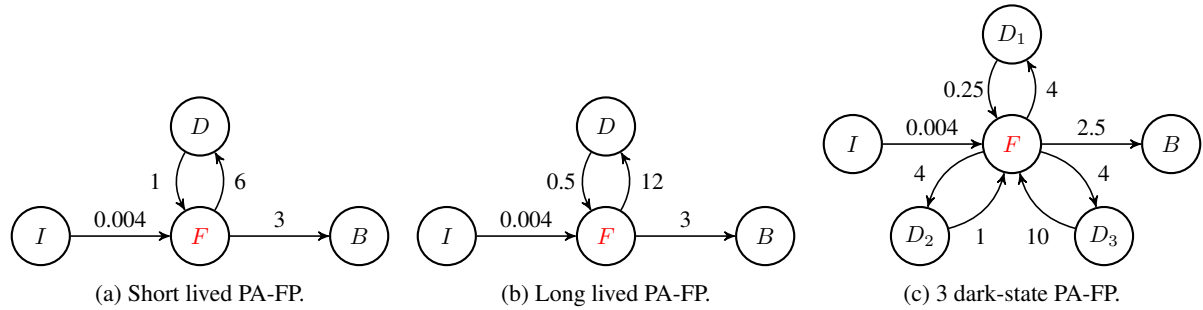


Figure 6: The three models of PA-FP photophysics considered in simulations.

CSR									
Short lived			Long lived			3 dark-states			
	Truth	Avg	Sd	Truth	Avg	Sd	Truth	Avg	Sd
$r_F \cdot 10^3$	4.000	3.984	0.226	4.000	4.045	0.257	4.000	3.992	0.235
r_B	3.000	3.080	0.223	3.000	3.0558	0.276	2.500	2.123	0.135
r_D	6.000	6.809	0.829	12.000	12.916	1.863	-	5.633	0.519
r_R	1.000	1.088	0.148	0.500	0.523	0.072	-	0.334	0.038
$\mathbb{E}[G]$	11.294	11.331	0.711	13.294	13.425	0.791	15.479	15.472	0.929
p	0.333	0.313	0.025	0.200	0.193	0.015	0.172	0.2745	0.021
$q_{0.25}$	0.160	0.157	0.009	0.760	0.904	0.104	0.440	0.321	0.065
$q_{0.50}$	1.120	1.239	0.109	4.920	5.073	0.368	4.160	4.526	0.293
$q_{0.75}$	3.360	3.518	0.304	12.000	12.291	0.908	12.240	12.389	0.810
$q_{0.99}$	13.800	13.907	0.952	45.480	44.976	2.317	50.041	48.286	2.350
Clusters									
Short lived			Long lived			3 dark-states			
	Truth	Avg	Sd	Truth	Avg	Sd	Truth	Avg	Sd
$r_F \cdot 10^3$	4.000	4.002	0.275	4.000	3.981	0.237	4.000	4.003	0.261
r_B	3.000	3.061	0.239	3.000	3.109	0.319	2.500	2.121	0.178
r_D	6.000	6.746	0.876	12.000	13.448	2.689	-	5.539	0.606
r_R	1.000	1.070	0.164	0.500	0.536	0.091	-	0.325	0.048
$\mathbb{E}[G]$	11.294	11.379	0.728	13.294	13.375	0.744	15.479	15.474	1.149
p	0.333	0.314	0.024	0.200	0.190	0.019	0.172	0.278	0.022
$q_{0.25}$	0.160	0.155	0.010	0.760	0.893	0.104	0.440	0.313	0.067
$q_{0.50}$	1.120	1.217	0.094	4.920	5.067	0.316	4.160	4.561	0.334
$q_{0.75}$	3.360	3.494	0.338	12.000	12.187	0.781	12.240	12.585	1.145
$q_{0.99}$	13.800	13.918	1.284	45.480	44.484	2.585	50.041	49.564	3.834
Fibers									
Short lived			Long lived			3 dark-states			
	Truth	Avg	Sd	Truth	Avg	Sd	Truth	Avg	Sd
$r_F \cdot 10^3$	4.000	4.001	0.252	4.000	4.029	0.243	4.000	4.036	0.247
r_B	3.000	3.095	0.214	3.000	3.163	0.305	2.500	2.084	0.152
r_D	6.000	6.835	0.925	12.000	13.657	2.117	-	5.465	0.516
r_R	1.000	1.084	0.154	0.500	0.538	0.076	-	0.322	0.039
$\mathbb{E}[G]$	11.294	11.282	0.656	13.294	13.246	0.866	15.48	15.677	1.008
p	0.333	0.314	0.026	0.200	0.190	0.016	0.172	0.277	0.020
$q_{0.25}$	0.160	0.163	0.008	0.760	0.922	0.139	0.440	0.317	0.059
$q_{0.50}$	1.120	1.233	0.078	4.920	5.120	0.409	4.160	4.600	0.292
$q_{0.75}$	3.360	3.481	0.253	12.000	12.255	1.031	12.240	12.694	0.927
$q_{0.99}$	13.800	13.838	0.843	45.480	44.595	2.344	50.041	50.738	3.424

Table 2: Results of fitting to 100 simulations from each combination of protein distribution (CSR, cluster, fibers) and PA-FP model (short lived, long lived, 3 dark-states).

7 Summary and discussion

In the present paper, we have established the IBCpp family of spatio-temporal clustered point processes, and we have provided results on the mark correlation functions for these models. Using an IBCpp particularly well-tailored to PALM data, the PALM-IBCpp, we described a procedure for estimation of parameters, allowing for a quantification of data artifacts. We considered a real dataset expressing LAT-mEos3.2 PA-FP, where the PALM-IBCpp model fit resulted in a close reconstruction of the spatio-temporal clustering behavior. From the refitting and simulation studies we saw that we can precisely estimate kinetic blinking rates under a variety of different protein and blinking conditions, and further provide valuable information about the number of reappearances and total lifetimes of PA-FP, even when the blinking model is misspecified.

The special structure of the mark correlation function in the IBCpp family allows the moment-based approach to be carried out on any arbitrary ROI, without having to specify a model for the proteins. This is perhaps the most important feature of our method, because it guarantees that the estimated kinetic rates are directly applicable to the ROI being analyzed. The well-known sensitivity of PA-FP photodynamics to the experimental conditions (Annibale et al. 2011b, Staudt et al. 2020) means that kinetic rates obtained via a calibration sample may not be entirely relevant in another sample, further emphasizing the importance of being able to directly estimate data artifacts from a given ROI.

As our focus has been on estimation on data artifacts, we opted for a simplified discretization scheme and kinetic photoswitching model in the PALM-IBCpp, and we used an estimation scheme based on functional data summaries and moment methods. Such tools are unlikely to be sufficient for fitting more complex descriptions of photoblinking, but on the other hand are fast to compute, and involve only low-dimensional optimization problems due to the step-wise procedure. As a result, it is possible to quickly analyze many ROI as part of a larger analysis, or for lowering the variance of the kinetic rate estimates by means of averaging.

Acknowledgements

This work was supported by the Centre for Stochastic Geometry and Advanced Bioimaging, funded by grant 8721 from the Villum Foundation. We acknowledge the use of the Nikon Imaging Facility (NIC) at King's College London for data acquisition.

Appendix A Moment results for IBCpp models

Let O be an IBCpp with motion-invariant protein process $\downarrow X$. Deriving the results of Section 3.2 is perhaps most easily done by taking as starting point the *f*-weighted second factorial moment measure, $\alpha_f^{(2)}$, given as

$$\alpha_f^{(2)}(A) = \mathbb{E} \left[\sum_{(o_1, t_{o_1}), (o_2, t_{o_2}) \in \downarrow O}^{\neq} \mathbb{1}_A(o_1, o_2) f(t_{o_1}, t_{o_2}) \right] \quad (\text{A.1})$$

for $A \in \mathbb{R}^d \times \mathbb{R}^d$ a Borel set. By use of a Cambell theorem we obtain

$$\alpha_f^{(2)}(A) = \int_A \left[\int f(t_{o_1}, t_{o_2}) dM_{O|(o_1, o_2)}^{(2)}(t_{o_1}, t_{o_2}) \right] d\alpha_O^{(2)}(o_1, o_2) \quad (\text{A.2})$$

so that, comparing the above with the definition of the mark correlation function, we get the alternative characterization

$$k_O^f(o_1, o_2) = \frac{1}{\int \int f(t_{o_1}, t_{o_2}) dM_{O|o_1}^{(1)}(t_{o_1}) dM_{O|o_2}^{(1)}(t_{o_2})} \frac{\partial \alpha_f^{(2)}}{\partial \alpha_O^{(2)}}(o_1, o_2) \quad (\text{A.3})$$

and we need merely compute the involved factors. We first compute the 1-point mark distributions. Let $A \subset \mathbb{R}^d$ and $B \subset \mathbb{R}_+$ be Borel sets, then we obtain

$$\Lambda_O(A \times B) = \mathbb{E} \left[\sum_{(x, t_x) \in X} \sum_{(y, t_y) \in Y_{(x, t_x)}} \mathbb{1}_A(y) \mathbb{1}_B(t_y) \right] + \mathbb{E} \left[\sum_{(e, t_e) \in E} \mathbb{1}_A(e) \mathbb{1}_B(t_e) \right] \quad (\text{A.4})$$

$$= \mathbb{E} \left[\sum_{(x, t_x) \in X} \sum_{i=1}^{|Y_{(x, t_x)}|} \mathbb{1}_A(x + \epsilon_i) \mathbb{1}_B(t_x + w_i) \right] + \mathbb{E} \left[\sum_{(e, t_e) \in E} \mathbb{1}_A(e) \mathbb{1}_B(t_e) \right] \quad (\text{A.5})$$

$$= \frac{\int \mathbb{E} \left[\sum_{i=1}^G \mathbb{1}_B(t_x + w_i) \right] dM_X^{(1)}(t_x)}{\mathbb{E}[G]} \int_A \lambda_Z dz + \int_B \frac{\mathbb{1}(t \in [0, b])}{b} dt \int_A \lambda_E de \quad (\text{A.6})$$

$$= \int_A \left[\eta \frac{\int \mathbb{E} \left[\sum_{i=1}^G \mathbb{1}_B(t_x + w_i) \right] dM_X^{(1)}(t_x)}{\mathbb{E}[G]} + (1 - \eta) \int_B \frac{\mathbb{1}(t \in [0, b])}{b} dt \right] d\Lambda_O(o) \quad (\text{A.7})$$

where we averaged out the ϵ_i , w_i , and t_x by conditioning on $\downarrow X$, when going from the second to the third line. From the above, we see that all involved mark distributions are independent of locations, with

$$M_Z^{(1)}(B) = \frac{\int \mathbb{E} \left[\sum_{i=1}^G \mathbb{1}_B(t_x + w_i) \right] dM_X^{(1)}(t_x)}{\mathbb{E}[G]} \quad (\text{A.8})$$

$$M_E^{(1)}(B) = \int_B \frac{\mathbb{1}(t \in [0, b])}{b} dt \quad (\text{A.9})$$

$$M_O^{(1)}(B) = \eta M_Z^{(1)}(B) + (1 - \eta) M_E^{(1)}(B) \quad (\text{A.10})$$

based on which the normalization for k_O^f is easily found

$$\int \int f(t_{o_1}, t_{o_2}) dM_O^{(1)}(t_{o_1}) dM_O^{(1)}(t_{o_2}) = \eta^2 \gamma_2(f) + (1 - \eta)^2 \gamma_2^E(f) + 2(1 - \eta) \eta \gamma_2^{EZ}(f) = \gamma_2^O(f) \quad (\text{A.11})$$

Next, we consider the second factorial moment measure of the typical cluster, $\alpha_{Y_{(x, t_x)}}^{(2)}$, which will be needed below. For arbitrary (x, t_x) and Borel sets $A \subset \mathbb{R}^d \times \mathbb{R}^d$, $B \subset \mathbb{R}_+ \times \mathbb{R}_+$, we have

$$\alpha_{Y_{(x, t_x)}}^{(2)}(A \times B) = \mathbb{E} \left[\sum_{(i, j)=1}^G \mathbb{1}(i \neq j) \mathbb{1}_A(x + \epsilon_i, x + \epsilon_j) \mathbb{1}_B(t_x + w_i, t_x + w_j) \right] \quad (\text{A.12})$$

$$= \mathbb{E} \left[\sum_{(i, j)=1}^G \mathbb{1}(i \neq j) \mathbb{1}_B(t_x + w_i, t_x + w_j) \right] \int_A h_\epsilon(x_1 - x) h_\epsilon(x_2 - x) d(x_1, x_2) \quad (\text{A.13})$$

obtained by averaging out the ϵ_i by conditioning on $(t_x, G, \{w_i\}_{i \in \mathbb{N}})$, from which follows

$$\alpha_{Y_{(x, t_x)}}^{(2)}(A) = \mathbb{E}[G(G-1)] \int_A h_\epsilon(x_1 - x) h_\epsilon(x_2 - x) d(x_1, x_2) \quad (\text{A.14})$$

$$M_{Y_{(x, t_x)}}^{(2)} = \frac{\mathbb{E} \left[\sum_{(i, j)=1}^G \mathbb{1}(i \neq j) \mathbb{1}_B(t_x + w_i, t_x + w_j) \right]}{\mathbb{E}[G(G-1)]} \quad (\text{A.15})$$

and we see that $M_{Y_{(x, t_x)}}^{(2)}$ is independent of x and, using a standard proof, we further obtain the identity in (15). The identity in (16) is obtained similarly, considering instead $(\Lambda_{Y_{(x, t_x)}})^2$. Finally, for the density of $\alpha_f^{(2)}$, we split the

summation according to the process memberships of each pair:

$$\alpha_f^{(2)}(A) = \mathbb{E} \left[\sum_{(x, t_x) \in X} \sum_{(i, j)=1}^{|Y_{(x, t_x)}|} \mathbb{1}(i \neq j) \mathbb{1}_A(x + \epsilon_i, x_2 + \epsilon_j) f(t_x + w_i, t_x + w_j) \right] \quad (\text{A.16})$$

$$+ \mathbb{E} \left[\sum_{(x_1, t_{x_1}), (x_2, t_{x_2}) \in X} \sum_{i=1}^{|Y_{(x_1, t_{x_1})}|} \sum_{j=1}^{|Y_{(x_2, t_{x_2})}|} \mathbb{1}_A(x_1 + \epsilon_i, x_2 + \epsilon'_j) f(t_{x_1} + w_i, t_{x_2} + w'_j) \right] \quad (\text{A.17})$$

$$+ \mathbb{E} \left[\sum_{(z, t_z) \in Z} \sum_{(e, t_e) \in E} \mathbb{1}_A(z, e) f(t_z, t_e) \right] + \mathbb{E} \left[\sum_{(z, t_z) \in Z} \sum_{(e, t_e) \in E} \mathbb{1}_A(e, z) f(t_e, t_z) \right] \quad (\text{A.18})$$

$$+ \mathbb{E} \left[\sum_{(e_1, t_{e_1}), (e_2, t_{e_2}) \in E} \mathbb{1}_A(e_1, e_2) f(t_{e_1}, t_{e_2}) \right] \quad (\text{A.19})$$

Using (A.14) and (A.15), recalling that E is a Poisson process independent of Z , and using that f is symmetrical, we see that

$$\alpha_f^{(2)}(A) = \gamma_1(f) \int \alpha_{\downarrow Y_{(0,0)}}^{(2)}(A - (x, x)) \lambda_{\downarrow X} dx \quad (\text{A.20})$$

$$+ \gamma_2(f) \int (\Lambda_{\downarrow Y_{(0,0)}})^2(A - (x_1, x_2)) d\alpha_{\downarrow X}^{(2)}(x_1, x_2) \quad (\text{A.21})$$

$$+ 2\gamma_2^{EZ}(f) \int_A \lambda_{\downarrow Z} \lambda_{\downarrow E} d(o_1, o_2) \quad (\text{A.22})$$

$$+ \gamma_2^E(f) \int_A \lambda_{\downarrow E}^2 d(o_1, o_2) \quad (\text{A.23})$$

$$= \gamma_1(f) \mathbb{E}[G(G-1)] \lambda_{\downarrow X} \int_A \int h_\epsilon(o_1 - x) h_\epsilon(o_2 - x) dx d(o_1, o_2) \quad (\text{A.24})$$

$$+ \gamma_2(f) \lambda_{\downarrow X}^2 \mathbb{E}[G]^2 \int_A \int g_{\downarrow X}(|x_1 - x_2|) h(o_1 - x_1) h(o_2 - x_2) d(x_1, x_2) d(o_1, o_2) \quad (\text{A.25})$$

$$+ 2\gamma_2^{EZ}(f) \lambda_{\downarrow Z} \lambda_{\downarrow E} \int_A d(o_1, o_2) \quad (\text{A.26})$$

$$+ \gamma_2^E(f) \lambda_{\downarrow E}^2 \int_A d(o_1, o_2) \quad (\text{A.27})$$

Write m for the Lebesgue measure on \mathbb{R}^d . Then, using the rotational symmetry of h_ϵ and $g_{\downarrow X}$, it follows that $\frac{\partial \alpha_f^{(2)}}{\partial m^2}(o_1, o_2)$ depends only on $r = ||o_1 - o_2||$, and

$$\frac{\partial \alpha_f^{(2)}}{\partial m^2}(r) = \gamma_1(f) n_c \lambda_{\downarrow Z} (h_\epsilon * h_\epsilon)(r) + \gamma_2(f) \lambda_{\downarrow Z}^2 (h_\epsilon * g_{\downarrow X})(r) + 2\gamma_2^{EZ}(f) \lambda_{\downarrow Z} \lambda_{\downarrow E} + \gamma_2^E(f) \lambda_{\downarrow E}^2 \quad (\text{A.28})$$

and in particular

$$\gamma_2^O(f) g_{\downarrow O} k_O^f(r) = \lambda_{\downarrow O}^{-2} \frac{\partial \alpha_f^{(2)}}{\partial m^2}(r) \quad (\text{A.29})$$

$$= \gamma_1(f) \frac{\eta}{\lambda_{\downarrow O}} n_c (h_\epsilon * h_\epsilon)(r) + \gamma_2(f) \eta^2 (h_\epsilon * g_{\downarrow X})(r) + 2\gamma_2^{EZ}(f) \eta (1 - \eta) + \gamma_2^E(f) (1 - \eta)^2 \quad (\text{A.30})$$

$$= \gamma_1(f) \frac{\eta}{\lambda_{\downarrow O}} n_c (h_\epsilon * h_\epsilon)(r) + \gamma_2(f) \eta^2 ((h_\epsilon * g_{\downarrow X})(r) - 1) + \gamma_2^O(f) \quad (\text{A.31})$$

which is (18), from which the remaining results of Section 3.2 follow easily as special cases of f and η .

Appendix B Approximate discretized statistics

B.1 Approximate $\phi(v)$

The mean value to compute is formally

$$\phi(v) := \frac{\mathbb{E} \left[\sum_{j_1, j_2 \in \{1, \dots, G\}}^{\neq} e^{iv|m_{j_1} - m_{j_2}|} \right]}{\mathbb{E} [G(G-1)]} \quad (\text{B.1})$$

where we have dropped the heavier notation of timepoints above, so that (m_{j_1}, m_{j_2}) are arrival times j_1 and j_2 in the typical blinking cluster. Denote by N_b the number of F -state visits (number of blinks), and by F_s the observed timepoints between the entrance to the s 'th and $(s+1)$ 'th F -state visits for $s < N_b$, and F_{N_b} are all observed timepoints after the last entrance to the F -state. Below, we will assume that $m_{j_1} < m_{j_2}$ for $(j_2 > j_1)$ when $(m_{j_1}, m_{j_2}) \in F_s$, that is, we have the arrival times sorted within each F_s set. We can split the summation according to whether m_{j_1} and m_{j_2} are from the same F_s , and otherwise how many F -state visits are separating them. Thus

$$\phi(v) = \frac{\mathbb{E} \left[\sum_{s=1}^{N_b} \sum_{(m_{j_1}, m_{j_2}) \in F_s}^{\neq} e^{iv|m_{j_1} - m_{j_2}|} \right]}{\mathbb{E} [G(G-1)]} \quad (\text{B.2})$$

$$+ \frac{\mathbb{E} \left[\sum_{s_1=1}^{N_b} \sum_{s_2=1}^{N_b} \mathbb{1}(s_1 \neq s_2) \sum_{m_{j_1} \in F_{s_1}} \sum_{m_{j_2} \in F_{s_2}} e^{iv|m_{j_1} - m_{j_2}|} \right]}{\mathbb{E} [G(G-1)]} \quad (\text{B.3})$$

To compute these terms, referred to as the "non-separated" and "separated" terms, respectively, we write the involved quantities in terms of a continuous part, and an error part, and demonstrate that the errors vanish asymptotically, and in particular can be ignored for a given framerate as a valid approximation.

First, we consider the number of timepoints in F_s , $|F_s|$. Since only those frames that do not fully overlap the signal from the s 'th F -visit (of which there are at most 2) cause discretization effects, we can write

$$|F_s| = \frac{W_{F_s}}{\Delta} + E_s^F \quad (\text{B.4})$$

where W_{F_s} is the waiting time that was spent on the s 'th visit to the F state, and E_s^F is an error term with

$$P(E_s^F \in (-1, 2)) = 1 \quad (\text{B.5})$$

and in particular, we obtain for G

$$G = \sum_{s=1}^{N_b} |F_s| = \sum_{s=1}^{N_b} \frac{W_{F_s}}{\Delta} + \sum_{s=1}^{N_b} E_s^F \quad (\text{B.6})$$

Next, consider the inner sum from the non-separated term:

$$\sum_{(m_{j_1}, m_{j_2}) \in F_s}^{\neq} e^{iv|m_{j_1} - m_{j_2}|} \quad (\text{B.7})$$

Here, note that the first observed timepoint in F_s , m_1^s , can be written as

$$m_1^s = E_s^{m_1} + W_I + \sum_{k=1}^{s-1} (W_{F_k} + W_{R_k}) \quad (\text{B.8})$$

since there is always a waiting time of W_I spent in the inactive state, and $(s-1)$ visits in and out of the F state before the s 'th visit. Here, $E_s^{m_1}$ is again a discretization error, with magnitude

$$P(E_s^{m_1} \in (0, \Delta)) = 1 \quad (\text{B.9})$$

Since each member of F_s is a whole number of Δ -increments away from m_1^s , this in particular means that, for $(m_{j_1}, m_{j_2}) \in F_s$ with $j_2 > j_1$:

$$|m_{j_1} - m_{j_2}| = (j_2 - j_1)\Delta \quad (\text{B.10})$$

and any discretization effects, and the time spent in the I -state, can be seen to disappear here. We can now expand on the non-separate term enumerator:

$$\mathbb{E} \left[\sum_{s=1}^{N_b} \sum_{(m_{j_1}, m_{j_2}) \in F_s}^{\neq} e^{iv|m_{j_1} - m_{j_2}|} \right] = \quad (\text{B.11})$$

$$\mathbb{E} \left[\sum_{s=1}^{N_b} \sum_{(j_1, j_2) \in \{1, 2, \dots, |F_s|\}}^{\neq} e^{iv(j_1 \vee j_2 - j_1 \wedge j_2)\Delta} \right] = \quad (\text{B.12})$$

$$2\mathbb{E} \left[\sum_{s=1}^{N_b} \sum_{j=1}^{|F_s|-1} (|F_s| - j) e^{ivj\Delta} \right] = \quad (\text{B.13})$$

$$2\mathbb{E} \left[\sum_{s=1}^{N_b} \frac{e^{iv\Delta(|F_s|-1)} + e^{-iv\Delta}(|F_s|-1) - |F_s|}{(e^{-iv\Delta} - 1)^2} \right] = \quad (\text{B.14})$$

$$2\mathbb{E} \left[\sum_{s=1}^{N_b} \frac{e^{ivW_{F_s}} e^{iv\Delta(E_s^F - 1)} + e^{-iv\Delta}(\frac{W_{F_s}}{\Delta} + E_s^F - 1) - \frac{W_{F_s}}{\Delta} - E_s^F}{(e^{-iv\Delta} - 1)^2} \right] \quad (\text{B.15})$$

At this point, consider what happens in the limit as $\Delta \rightarrow 0$ for the complete non-separate term:

$$\lim_{\Delta \rightarrow 0} \frac{\mathbb{E} \left[\sum_{s=1}^{N_b} \sum_{(m_{j_1}, m_{j_2}) \in F_s}^{\neq} e^{iv|m_{j_1} - m_{j_2}|} \right]}{\mathbb{E} [G(G-1)]} = \quad (\text{B.16})$$

$$\frac{2\mathbb{E} \left[\lim_{\Delta \rightarrow 0} \sum_{s=1}^{N_b} e^{ivW_{F_s}} e^{iv\Delta(E_s^F - 1)} + \frac{W_{F_s}}{\Delta} (e^{-iv\Delta} - 1) + E_s^F (e^{-iv\Delta} - 1) - e^{-iv\Delta} \right]}{\lim_{\Delta \rightarrow 0} (e^{-iv\Delta} - 1)^2 \left[\mathbb{E} \left[\left(\sum_{s=1}^{N_b} \frac{W_{F_s}}{\Delta} + \sum_{s=1}^{N_b} E_s^F \right)^2 \right] - \mathbb{E} \left[\sum_{s=1}^{N_b} \frac{W_{F_s}}{\Delta} + \sum_{s=1}^{N_b} E_s^F \right] \right]} = \quad (\text{B.17})$$

$$\frac{2\mathbb{E} \left[\sum_{s=1}^{N_b} 1 + ivW_{F_s} - e^{iW_{F_s}} \right]}{v^2 \mathbb{E} \left[\left(\sum_{s=1}^{N_b} W_{F_s} \right)^2 \right]} = \quad (\text{B.18})$$

$$\frac{2\mathbb{E} [N_b] (1 + iv\mathbb{E} [W_F] - \phi_F(u))}{v^2 (\mathbb{E} [N_b] \mathbb{E} [W_F^2] + \mathbb{E} [N_b(N_b-1)] \mathbb{E} [W_F]^2)} \quad (\text{B.19})$$

Predictably the rounding errors play no role in the limit, and as a simple approximation we therefore set $E_s^F = \frac{1}{2}$ to the midpoint of its domain for all s , to obtain the asymptotically exact approximation:

$$\frac{\mathbb{E} \left[\sum_{s=1}^{N_b} \sum_{(m_{j_1}, m_{j_2}) \in F_s}^{\neq} e^{iv|m_{j_1} - m_{j_2}|} \right]}{\mathbb{E} [G(G-1)]} \approx \quad (\text{B.20})$$

$$\frac{2\mathbb{E} \left[\sum_{s=1}^{N_b} e^{ivW_{F_s}} e^{-iv\Delta \frac{1}{2}} + e^{-iv\Delta} (\frac{W_{F_s}}{\Delta} - \frac{1}{2}) - \frac{W_{F_s}}{\Delta} - \frac{1}{2} \right]}{(e^{-iv\Delta} - 1)^2 \left[\mathbb{E} \left[\left(\sum_{s=1}^{N_b} \frac{W_{F_s}}{\Delta} + \frac{1}{2} \right)^2 \right] - \mathbb{E} \left[\sum_{s=1}^{N_b} \frac{W_{F_s}}{\Delta} + \frac{1}{2} \right] \right]} = \quad (\text{B.21})$$

$$\frac{2\mathbb{E} [N_b] (\phi_F(v) e^{-iv\frac{1}{2}} + e^{-iv\Delta} (\frac{\mathbb{E}[W_F]}{\Delta} - \frac{1}{2}) - \frac{\mathbb{E}[W_F]}{\Delta} - \frac{1}{2})}{(e^{-iv\Delta} - 1)^2 \left(\mathbb{E} [N_b^2] \left(\frac{\mathbb{E}[W_F]}{\Delta} + \frac{1}{2} \right)^2 + \mathbb{E} [N_b] \left[\frac{\mathbb{E}[W_F^2] - \mathbb{E}[W_F]^2}{\Delta^2} - \frac{\mathbb{E}[W_F]}{\Delta} - \frac{1}{2} \right] \right)} \quad (\text{B.22})$$

which is $\frac{A(v)}{D}$.

Now, consider the separate summation enumerator. We use similar techniques as before. Note that for F_{s_1} and F_{s_2} there are $|s_1 - s_2 - 1| W_F$ waiting times, and $|s_1 - s_2| W_R$ waiting times, separating the closest pair in $F_{s_1} \times F_{s_2}$, up to rounding error. Thus, if we enumerate the timepoints in F_{s_1} instead starting from the end (so that $m'_j \in F_{s_1}$ is the j 'th largest value in F_s , $j \geq 1$), the differences in timepoints $m'_{j_1} \in F_{s_1}$ and $m_{j_2} \in F_{s_2}$, with $s_2 > s_1$, can be written on the form.

$$|m'_{j_1} - m_{j_2}| = W_{s_2} + \sum_{k=1}^{s_2 - s_1} (W_{R_{s_1+k}} + W_{F_{s_1+k}}) + (j_1 + j_2 - 2)\Delta + E_{(s_1, s_2)} \quad (\text{B.23})$$

where $E_{(s_1, s_2)}$ only depends on (s_1, s_2) and has

$$P(E_{(s_1, s_2)} \in (-\Delta, \Delta)) = 1 \quad (\text{B.24})$$

Therefore:

$$\sum_{s_1=1}^{N_b} \sum_{s_2=1}^{N_b} \mathbb{1}(s_1 \neq s_2) \sum_{m_{j_1} \in F_{s_1}} \sum_{m_{j_2} \in F_{s_2}} e^{iv|m_{j_1} - m_{j_2}|} = \quad (\text{B.25})$$

$$2 \sum_{s_1=1}^{N_b-1} \sum_{s_2=s_1+1}^{N_b} \sum_{m_{j_1} \in F_{s_1}} \sum_{m_{j_2} \in F_{s_2}} e^{iv|m_{j_1} - m_{j_2}|} = \quad (\text{B.26})$$

$$2 \sum_{s_1=1}^{N_b-1} \sum_{s_2=s_1+1}^{N_b} e^{ivW_{s_2}} e^{iv \sum_{k=1}^{s_2-s_1} (W_{R_{s_1+k}} + W_{F_{s_1+k}})} e^{ivE_{(s_1, s_2)}} e^{-iv\Delta 2} \sum_{j_1=1}^{|F_{s_1}|} \sum_{j_2=1}^{|F_{s_2}|} e^{iv(j_1 + j_2)\Delta} = \quad (\text{B.27})$$

$$2 \sum_{s_1=1}^{N_b-1} \sum_{s_2=s_1+1}^{N_b} e^{ivW_{s_2}} e^{iv \sum_{k=1}^{s_2-s_1} (W_{R_{s_1+k}} + W_{F_{s_1+k}})} e^{ivE_{(s_1, s_2)}} e^{-iv\Delta 2} \frac{(e^{iv\Delta|F_{s_1}|} - 1)(e^{iv\Delta|F_{s_2}|} - 1)}{(e^{iv\Delta} - 1)^2} \quad (\text{B.28})$$

At this point, it should be clear that discretization effects again have no impact in the limit. For the sake of completion, we compute also this asymptotic value:

$$\lim_{\Delta \rightarrow 0} \frac{\mathbb{E} \left[\sum_{s_1=1}^{N_b} \sum_{s_2=1}^{N_b} \mathbb{1}(s_1 \neq s_2) \sum_{m_{j_1} \in F_{s_1}} \sum_{m_{j_2} \in F_{s_2}} e^{iv|m_{j_1} - m_{j_2}|} \right]}{\mathbb{E} [G(G-1)]} = \quad (\text{B.29})$$

$$\frac{-\mathbb{E} \left[2 \sum_{s_1=1}^{N_b-1} \sum_{s_2=s_1+1}^{N_b} e^{ivW_{s_2}} e^{iv \sum_{k=1}^{s_2-s_1} (W_{R_{s_1+k}} + W_{F_{s_1+k}})} (e^{ivW_{F_{s_1}}} - 1)(e^{ivW_{F_{s_2}}} - 1) \right]}{v^2 (\mathbb{E} [N_b] \mathbb{E} [W_F^2] + \mathbb{E} [N_b(N_b-1)] \mathbb{E} [W_F]^2)} = \quad (\text{B.30})$$

$$\frac{2 \left(\frac{\phi_F(v)-1}{\phi_{(F+R)}(v)-1} \right)^2 \phi_R(v) (1 + \mathbb{E} [N_b] (\phi_{(F+R)}(v) - 1) - \mathbb{E} [\phi_{(F+R)}(v)^{N_b}])}{v^2 (\mathbb{E} [N_b] \mathbb{E} [W_F^2] + \mathbb{E} [N_b(N_b-1)] \mathbb{E} [W_F]^2)} \quad (\text{B.31})$$

Thus, replacing again all discretization errors with the midpoints of their domains ($E_s^F = \frac{1}{2}$, $E_{s_1, s_2} = 0$), we get an asymptotically exact approximation:

$$\frac{\mathbb{E} \left[\sum_{s_1=1}^{N_b} \sum_{s_2=1}^{N_b} \mathbb{1}(s_1 \neq s_2) \sum_{m_{j_1} \in F_{s_1}} \sum_{m_{j_2} \in F_{s_2}} e^{iv|m_{j_1} - m_{j_2}|} \right]}{\mathbb{E} [G(G-1)]} \approx \quad (\text{B.32})$$

$$\frac{2e^{-iv\Delta 2} \mathbb{E} \left[\sum_{s_1=1}^{N_b-1} \sum_{s_2=s_1+1}^{N_b} e^{ivW_{s_2}} e^{iv \sum_{k=1}^{s_2-s_1} (W_{R_{s_1+k}} + W_{F_{s_1+k}})} (e^{ivW_{F_{s_1}}} e^{iv\Delta \frac{1}{2}} - 1)(e^{ivW_{F_{s_2}}} e^{iv\Delta \frac{1}{2}} - 1) \right]}{(e^{-iv\Delta} - 1)^2 \left(\mathbb{E} [N_b^2] \left(\frac{\mathbb{E} [W_F]}{\Delta} + \frac{1}{2} \right)^2 + \mathbb{E} [N_b] \left[\frac{\mathbb{E} [W_F^2] - \mathbb{E} [W_F]^2}{\Delta^2} - \frac{\mathbb{E} [W_F]}{\Delta} - \frac{1}{2} \right] \right)} = \quad (\text{B.33})$$

$$\frac{2e^{-iv\Delta 2} \left(\frac{\phi_F(v)e^{iv\Delta \frac{1}{2}} - 1}{\phi_{(F+R)}(v) - 1} \right)^2 \phi_R(v) (\mathbb{E} [\phi_{(F+R)}(v)^{N_b}] - 1 - \mathbb{E} [N_b] (\phi_{(F+R)}(v) - 1))}{(e^{-iv\Delta} - 1)^2 \left(\mathbb{E} [N_b^2] \left(\frac{\mathbb{E} [W_F]}{\Delta} + \frac{1}{2} \right)^2 + \mathbb{E} [N_b] \left[\frac{\mathbb{E} [W_F^2] - \mathbb{E} [W_F]^2}{\Delta^2} - \frac{\mathbb{E} [W_F]}{\Delta} - \frac{1}{2} \right] \right)} \quad (\text{B.34})$$

which is $\frac{B(v)C(v)}{D}$.

B.2 Approximate n_c

We wish to compute

$$n_c = \frac{\mathbb{E} [G^2]}{\mathbb{E} [G]} - 1 \quad (\text{B.35})$$

Instead of approximating the moments directly, we first approximate the distribution of G , from which the moments can be obtained. We can write somewhat loosely

$$G = \sum_{s=1}^{N_b} \#(\text{frames hit by the } s\text{'th F-signal}) - \sum_{s=1}^{N_b-1} \mathbb{1}(\text{F-signals } s \text{ and } s+1 \text{ share a frame}) \quad (\text{B.36})$$

where by "sharing" we mean that the continuous time signals emitted from the $2 F$ -state visits hit the same frame. Now, computing the distribution of G from this representation is made intractable due to the dependence and complicated behavior in the summands caused by discretization to the fixed grid ΔZ . Instead, we replace the summands with their mean under discretization to grids $\Delta Z + U$, where $U \sim \text{Uni}(0, \Delta)$. Write $\mathbb{E}_U[\cdot]$ for this mean, and let $\lfloor a \rfloor$ and $\{a\}$ denote the integer and fractional parts, respectively, of a number a . Write T_s^I and T_s^O for the entrance and exit times, respectively, for the s 'th F -state visit, and D_s for the distance from T_s^I to the nearest gridpoint larger than T_s^I . Then, we obtain for any s

$$\mathbb{E}_U[\#(\text{frames hit by the } s\text{'th F-signal})] = \quad (\text{B.37})$$

$$\lfloor W_{F_s} \Delta^{-1} \rfloor + \mathbb{E}_U[\mathbb{1}(D_s < \{W_{F_s} \Delta^{-1}\}) + \mathbb{1}(D_s > \{W_{F_s} \Delta^{-1}\})] = \quad (\text{B.38})$$

$$\lfloor W_{F_s} \Delta^{-1} \rfloor + 2\{W_{F_s} \Delta^{-1}\} + (1 - \{W_{F_s} \Delta^{-1}\}) = \quad (\text{B.39})$$

$$W_{F_s} \Delta^{-1} + 1 \quad (\text{B.40})$$

Now, for the second sum, we get

$$\mathbb{E}_U[\mathbb{1}(\text{F-signals } s \text{ and } s+1 \text{ share a frame})] = \quad (\text{B.41})$$

$$1 - \mathbb{E}_U[\mathbb{1}(\text{there is a gridpoint between } T_s^O \text{ and } T_{s+1}^I)] = \quad (\text{B.42})$$

$$1 - (W_{R_s} \Delta^{-1} \mathbb{1}(W_{R_s} \leq \Delta) + \mathbb{1}(W_{R_s} > \Delta)) = \quad (\text{B.43})$$

$$\mathbb{1}(W_{R_s} \Delta^{-1} \leq 1)(1 - W_{R_s} \Delta^{-1}) \quad (\text{B.44})$$

and our approximation for G is thus

$$G \approx \sum_{s=1}^{N_b} \frac{W_{F_s}}{\Delta} + 1 - \sum_{s=1}^{N_b-1} \mathbb{1}\left(\frac{W_{R_s}}{\Delta} \leq 1\right)(1 - \frac{W_{R_s}}{\Delta}) \quad (\text{B.45})$$

from which we obtain

$$\mathbb{E}[G] \approx \mathbb{E}[N_b] \left(\frac{\mathbb{E}[W_F]}{\Delta} + 1 \right) - \mathbb{E}[N_b - 1] \mu_R^1 \quad (\text{B.46})$$

where $\mu_R^1 = \int_0^1 (1-x) dP_{\underline{W}_R}(x)$, and

$$\mathbb{E}[G^2] \approx \mathbb{E}[N_b^2] \left(\frac{\mathbb{E}[W_F]}{\Delta} + 1 \right)^2 + \mathbb{E}[N_b] \frac{\mathbb{E}[W_F^2] - \mathbb{E}[W_F]^2}{\Delta^2} \quad (\text{B.47})$$

$$+ \mathbb{E}[(N_b - 1)^2] (\mu_R^1)^2 + \mathbb{E}[N_b - 1] (\mu_R^2 - (\mu_R^1)^2) \quad (\text{B.48})$$

$$- 2\mathbb{E}[N_b(N_b - 1)] \left(\frac{\mathbb{E}[W_F]}{\Delta} + 1 \right) \mu_R^1 \quad (\text{B.49})$$

with $\mu_R^2 = \int_0^1 (1-x)^2 dP_{\underline{W}_R}(x)$.

If we write $n_c(\Delta)$ for the approximation of n_c given a framerate of Δ^{-1} , we have that $n_c(\Delta)$ is asymptotically exact in the sense that, after appropriate normalization, we have

$$\lim_{\Delta \rightarrow 0} \Delta n_c(\Delta) = \lim_{\Delta \rightarrow 0} \Delta n_c \quad (\text{B.50})$$

where this asymptotic value is given as

$$\lim_{\Delta \rightarrow 0} \Delta n_c = \frac{\mathbb{E}[N_b] \mathbb{E}[W_F^2] + \mathbb{E}[N_b(N_b - 1)] \mathbb{E}[W_F]^2}{\mathbb{E}[N_b] \mathbb{E}[W_F]} \quad (\text{B.51})$$

B.3 Approximate $\gamma_2(d)$

By definition, we have

$$\gamma_2(d) = \frac{\mathbb{E} \left[\sum_{k=1}^G \sum_{j=1}^{G'} d(m_k, m'_j) \right]}{\mathbb{E} [G]^2} = \frac{\mathbb{E} \left[\sum_{k=1}^G \sum_{j=1}^{G'} m_k + m'_j \right]}{\mathbb{E} [G]^2} \quad (\text{B.52})$$

where we again drop the heavier time point notation, such that e.g. m_k is arrival time k in a typical cluster, and m'_j is mark j in an independent copy of the typical cluster. Clearly, then,

$$\frac{1}{2} \gamma_2(d) = \frac{\mathbb{E} \left[\sum_{k=1}^G m_k \right]}{\mathbb{E} [G]} \quad (\text{B.53})$$

Now, write T_s^I for the (continuous) entrance time to the s 'th F -state visit. Then the first observed timepoint in F_s can be written as $T_s^I + E_s$, where E_s is a discretization error with $P(0 \leq E_s \leq \Delta) = 1$. Note further, that

$$T_s^I = W_I + \sum_{i=1}^{s-1} (W_{F_i} + W_{R_i}) \quad (\text{B.54})$$

and we arrive at the expression

$$\frac{1}{2} \gamma_2(d) = \frac{\mathbb{E} \left[\sum_{s=1}^{N_b} |F_s| (T_s^I + E_s) + \sum_{k=1}^{|F_s|} k \Delta \right]}{\mathbb{E} [G]} \quad (\text{B.55})$$

$$= \frac{\mathbb{E} \left[\sum_{s=1}^{N_b} |F_s| (T_s^I + E_s) \right]}{\mathbb{E} [G]} + \frac{\Delta \mathbb{E} \left[\sum_{s=1}^{N_b} |F_s| (|F_s| + 1) \right]}{2 \mathbb{E} [G]} \quad (\text{B.56})$$

Now, setting everywhere $|F_s| = \frac{W_{F_s}}{\Delta} + \frac{1}{2}$ as in Appendix B.1, and similarly setting all $E_s = \Delta \frac{1}{2}$, we get

$$\frac{\mathbb{E} \left[\sum_{s=1}^{N_b} \sum_{k=1}^{|F_s|} k \Delta \right]}{\mathbb{E} [G]} = \frac{\mathbb{E} [N_b] \left(\frac{\mathbb{E} [W_F^2]}{2\Delta} + \mathbb{E} [W_F] + \frac{3\Delta}{8} \right)}{\mathbb{E} [G]} \quad (\text{B.57})$$

and

$$\frac{\mathbb{E} \left[\sum_{s=1}^{N_b} |F_s| (T_s^I + E_s) \right]}{\mathbb{E} [G]} = \mathbb{E} [W_I] + \frac{\mathbb{E} \left[\sum_{s=1}^{N_b} \left(\frac{W_{F_s}}{\Delta} + \frac{1}{2} \right) \left(\sum_{i=1}^{s-1} (W_{F_i} + W_{R_i}) + \Delta \frac{1}{2} \right) \right]}{\mathbb{E} [G]} \quad (\text{B.58})$$

$$= \mathbb{E} [W_I] + \frac{\left(\frac{\mathbb{E} [W_F]}{\Delta} + \frac{1}{2} \right) \left(\frac{1}{2} \mathbb{E} [N_b (N_b - 1)] (\mathbb{E} [W_F] + \mathbb{E} [W_R]) + \mathbb{E} [N_b] \Delta \frac{1}{2} \right)}{\mathbb{E} [G]} \quad (\text{B.59})$$

so that setting $\mathbb{E} [G] \approx \mathbb{E} [N_b] \left(\frac{\mathbb{E} [W_F]}{\Delta} + \frac{1}{2} \right)$ yields the approximation. Again, the approximation is asymptotically exact, with limiting value

$$\lim_{\Delta \rightarrow 0} \frac{1}{2} \gamma_2(d) = \mathbb{E} [W_I] + \frac{\mathbb{E} [W_F] \left(\frac{1}{2} \mathbb{E} [N_b (N_b - 1)] (\mathbb{E} [W_F] + \mathbb{E} [W_R]) \right)}{\mathbb{E} [N_b] \mathbb{E} [W_F]} + \frac{\mathbb{E} [W_F^2]}{2 \mathbb{E} [W_F]} \quad (\text{B.60})$$

Appendix C Use on general $\downarrow X$

For general $\downarrow X$, we can nevertheless use the estimation procedures of Section 4 and obtain meaningful estimates. To see why this is true, we consider the means of standard kernel-estimators used above.

Assume again that the IBCpp O is observed in $W \times [0, b]$. Standard estimators of $\gamma_2^O(f) k_O^f$ and g_O , when O is motion-invariant, are given as

$$\hat{\gamma}_2^O(f) k_O^f(r) = \frac{\sum_{i \neq j} f(t_{o_i}, t_{o_j}) \kappa(||o_i - o_j|| - r) w(o_i, o_j)}{\sum_{i \neq j} \kappa(||o_i - o_j|| - r) w(o_i, o_j)} \quad (\text{C.1})$$

$$\hat{g}_O(r) = c(r) \sum_{i \neq j} \kappa(||o_i - o_j|| - r) w(o_i, o_j) \quad (\text{C.2})$$

Here, $c(r) = (2\pi r)^{-1} N^{-2} |W|$, κ is a smoothing kernel, and $w(x, y)$ are edge correction weights, see e.g. (Gelfand et al. 2010, p. 308, 393). We think of the sum as running over all observed pairs in O , and for simplicity the w are just indicator functions that the location pairs are in W^2 . The kernel and weights should be chosen identical for both estimators, as indicated by the notation. Our estimator of \hat{S}_O^f is then

$$\hat{S}_O^f(r) = \hat{g}_O(r) \hat{\gamma}_2^O(f) \hat{k}_O^f(r) = c(r) \sum_{i \neq j} f(t_{o_i}, t_{o_j}) \kappa(|o_i - o_j| - r) w(o_i, o_j) \quad (\text{C.3})$$

Now, rather than computing the mean of \hat{S}_O^f directly, we write $\tilde{c}(r) = N^2 c(r)$, and compute the mean of $N^2 \hat{S}_O^f(r)$, which yields slightly more elegant computations. By splitting the summation according to the cluster and process relationships of pairs, and using the symmetry of f , we obtain

$$\mathbb{E} \left[N^2 \hat{S}_O^f(r) \right] = \mathbb{E} \left[\tilde{c}(r) \sum_{(x, t_x) \in X} \sum_{(y_1, t_{y_1}), (y_2, t_{y_2}) \in Y_{(x, t_x)}}^{\neq} f(t_{y_1}, t_{y_2}) \kappa(|y_1 - y_2| - r) w(y_1, y_2) \right] \quad (\text{C.4})$$

$$+ \mathbb{E} \left[\tilde{c}(r) \sum_{(x_1, t_{x_1}), (x_2, t_{x_2}) \in X}^{\neq} \sum_{(y_1, t_{y_1}) \in Y_{(x_1, t_{x_1})}} \sum_{(y_2, t_{y_2}) \in Y_{(x_2, t_{x_2})}} f(t_{y_1}, t_{y_2}) \kappa(|y_1 - y_2| - r) w(y_1, y_2) \right] \quad (\text{C.5})$$

$$+ 2 \mathbb{E} \left[\tilde{c}(r) \sum_{(x, t_x) \in X} \sum_{(y, t_y) \in Y_{(x, t_x)}} \sum_{(e, t_e) \in E} f(t_y, t_e) \kappa(|y - e| - r) w(y, e) \right] \quad (\text{C.6})$$

$$+ \mathbb{E} \left[\tilde{c}(r) \sum_{(e_1, t_{e_1}), (e_2, t_{e_2}) \in E}^{\neq} f(t_{e_1}, t_{e_2}) \kappa(|e_1 - e_2| - r) w(e_1, e_2) \right] \quad (\text{C.7})$$

Using the independence structures of our model, we average out the clusters to arrive at

$$\mathbb{E} \left[N^2 \hat{S}_O^f(r) \right] = \gamma_1(f) n_c \mathbb{E} [G] \mathbb{E} \left[\tilde{c}(r) \sum_{(x, t_x) \in X} (h_\epsilon * h_\epsilon)_x^{w, \kappa}(r) \right] \quad (\text{C.8})$$

$$+ \gamma_2(f) \mathbb{E} [G]^2 \mathbb{E} \left[\tilde{c}(r) \sum_{(x_1, t_{x_1}), (x_2, t_{x_2}) \in X}^{\neq} (h_\epsilon * h_\epsilon)_{x_1, x_2}^{w, \kappa}(r) \right] \quad (\text{C.9})$$

$$+ 2 \gamma_2^{EZ}(f) \mathbb{E} [G] \lambda_{\downarrow E} \mathbb{E} \left[\tilde{c}(r) \sum_{(x, t_x) \in X} (h_\epsilon * h_\epsilon)_x^{w, \kappa}(r) \right] \quad (\text{C.10})$$

$$+ \gamma_2^E(f) \lambda_{\downarrow E}^2 \mathbb{E} [\tilde{c}(r) (h_\epsilon * h_\epsilon)_x^{w, \kappa}(r)] \quad (\text{C.11})$$

where

$$(h_\epsilon * h_\epsilon)_x^{w, \kappa}(r) = \int \kappa(|t_1 - t_2| - r) h_\epsilon(t_1) h_\epsilon(t_2) \mathbb{1}_{W^2}(x + t_1, x + t_2) dt_1 dt_2 \quad (\text{C.12})$$

$$(h_\epsilon * h_\epsilon)_{x_1, x_2}^{w, \kappa}(r) = \int \kappa(|t_1 + x_1 - t_2 - x_2| - r) h_\epsilon(t_1) h_\epsilon(t_2) \mathbb{1}_{W^2}(x_1 + t_1, x_2 + t_2) dt_1 dt_2 \quad (\text{C.13})$$

$$(h_\epsilon * h_\epsilon)_x^{w, \kappa}(r) = \int \kappa(|x + t_1 - t_2| - r) h_\epsilon(t_1) \mathbb{1}_{W^2}(x + t_1, t_2) dt_1 dt_2 \quad (\text{C.14})$$

$$(h_\epsilon * h_\epsilon)_x^{w, \kappa}(r) = \int \kappa(|t_1 - t_2| - r) \mathbb{1}_{W^2}(t_1, t_2) dt_1 dt_2 \quad (\text{C.15})$$

By considering what happens for $f = 1$ (in which case $\gamma_1(f) = \gamma_2(f) = \gamma_2^E(f) = \gamma_2^{EZ}(f) = 1$), we see that we can rewrite the above as

$$\mathbb{E} \left[N^2 \hat{S}_O^f(r) \right] = (\gamma_1(f) - \gamma_2(f)) n_c \mathbb{E}[G] \mathbb{E} \left[\tilde{c}(r) \sum_{x \in \downarrow X} (h_\epsilon * h_\epsilon)_x^{w,\kappa}(r) \right] \quad (\text{C.16})$$

$$+ \gamma_2(f) \mathbb{E} \left[N^2 \hat{g}_O(r) \right] \quad (\text{C.17})$$

$$+ 2(\gamma_2^{EZ}(f) - \gamma_2(f)) \mathbb{E}[G] \lambda_{\downarrow E} \mathbb{E} \left[\tilde{c}(r) \sum_{x \in \downarrow X} (h_\epsilon * h_\epsilon)_x^{w,\kappa}(r) \right] \quad (\text{C.18})$$

$$+ (\gamma_2^E(f) - \gamma_2(f)) \lambda_{\downarrow E}^2 \mathbb{E} \left[\tilde{c}(r) (h_\epsilon * h_\epsilon)_x^{w,\kappa}(r) \right] \quad (\text{C.19})$$

and we already have a very similar expression to the motion-invariant case. The obstacle to further exact computations come from edge and kernel smoothing biases. For the pure cluster term, consider first $x \in \downarrow X$ which is positioned centrally in W , such that the edge correction weights can be disregarded. Then we would have

$$(h_\epsilon * h_\epsilon)_x^{w,\kappa}(r) \approx \int \kappa(\|t_1 - t_2\| - r) h_\epsilon(t_1) h_\epsilon(t_2) dt_1 dt_2 \quad (\text{C.20})$$

$$= \int \kappa(\|t_1\| - r) h_\epsilon(t_1 + t_2) dt_1 h_\epsilon(t_2) dt_2 \quad (\text{C.21})$$

$$= \int l \kappa(l - r) h_\epsilon(l [\cos(\theta), \sin(\theta)] + t_2) dl d\theta h_\epsilon(t_2) dt_2 \quad (\text{C.22})$$

$$= 2\pi \int l \kappa(l - r) (h_\epsilon * h_\epsilon)(l) dl \quad (\text{C.23})$$

obtained by polar integration. Thus, for central x , we have a kernel-smoothed version of the cluster autoconvolution. For x closer to the border of W (on either side), not all pairs will be considered. As a simple approximation for all x , we therefore assume an edge-affected cluster contributes the same as a central cluster, but weighted with the expected fraction of points observed in W , $\int_{W-x} h_\epsilon(t) dt$, so that

$$\mathbb{E}[G] \mathbb{E} \left[\tilde{c}(r) \sum_{x \in \downarrow X} (h_\epsilon * h_\epsilon)_x^{w,\kappa}(r) \right] \approx \frac{|W| \Lambda_Z(W)}{r} \int l \kappa(l - r) (h_\epsilon * h_\epsilon)(l) dl \quad (\text{C.24})$$

In particular, for small kernel bandwidths, we have

$$\mathbb{E}[G] \mathbb{E} \left[\tilde{c}(r) \sum_{x \in \downarrow X} (h_\epsilon * h_\epsilon)_x^{w,\kappa}(r) \right] \approx |W| \Lambda_Z(W) (h_\epsilon * h_\epsilon)(r) \quad (\text{C.25})$$

Using the same tricks for the mixed term, we have for central x

$$(h_\epsilon * h_\epsilon)_x^{w,\kappa}(r) \approx \int \kappa(\|x + t_1 - t_2\| - r) h_\epsilon(t_1) dt_1 dt_2 \quad (\text{C.26})$$

$$= \int \kappa(\|t_2\| - r) dt_2 \int h_\epsilon(t_1) dt_1 \quad (\text{C.27})$$

so that, for small kernel bandwidths and all x , we have

$$\mathbb{E}[G] \mathbb{E} \left[\tilde{c}(r) \sum_{x \in \downarrow X} (h_\epsilon * h_\epsilon)_x^{w,\kappa}(r) \right] \approx |W| \Lambda_Z(W) \quad (\text{C.28})$$

Finally, for the pure noise term, note that

$$\lambda_{\downarrow E}^2 \mathbb{E} \left[\tilde{c}(r) (h_\epsilon * h_\epsilon)_x^{w,\kappa}(r) \right] = \mathbb{E} \left[|E \cap W|^2 \hat{g}_E(r) \right] \quad (\text{C.29})$$

where $\hat{g}_E(r)$ is the estimator of the pair correlation function of a stationary Poisson process, so that we can reasonably expect

$$\lambda_{\downarrow E}^2 \mathbb{E} \left[\tilde{c}(r) (h_\epsilon * h_\epsilon)_x^{w,\kappa}(r) \right] \approx \mathbb{E} \left[|E \cap W|^2 \right] \quad (\text{C.30})$$

Thus, assuming the kernel bandwidth is small, and the majority of points in $\downarrow X$ are not close to the boundary of W relative to the effective cluster size, we obtain

$$\mathbb{E} \left[N^2 \hat{S}_O^f(r) \right] \approx (\gamma_1(f) - \gamma_2(f)) n_c |W| \Lambda_Z(W) (h_\epsilon * h_\epsilon)(r) \quad (C.31)$$

$$+ \gamma_2(f) \mathbb{E} \left[N^2 \hat{g}_O(r) \right] \quad (C.32)$$

$$+ 2(\gamma_2^{EZ}(f) - \gamma_2(f)) \Lambda_E(W) \Lambda_Z(W) \quad (C.33)$$

$$+ (\gamma_2^E(f) - \gamma_2(f)) \mathbb{E} [|E \cap W|^2] \quad (C.34)$$

Finally, using simple Taylor approximations for the mean values, we have

$$\mathbb{E} \left[\hat{S}_O^f(r) \right] \approx (\gamma_1(f) - \gamma_2(f)) n_c \frac{\eta(W)}{\Lambda_O(W) |W|^{-1}} (h_\epsilon * h_\epsilon)(r) \quad (C.35)$$

$$+ \gamma_2(f) \mathbb{E} \left[\hat{g}_O(r) \right] \quad (C.36)$$

$$+ 2(\gamma_2^{EZ}(f) - \gamma_2(f)) \eta(W) (1 - \eta(W)) \quad (C.37)$$

$$+ (\gamma_2^E(f) - \gamma_2(f)) (1 - \eta(W))^2 \quad (C.38)$$

or

$$\mathbb{E} \left[\hat{S}_O^f(r) \right] \approx (\gamma_1(f) - \gamma_2(f)) n_c \frac{\eta(W)}{\Lambda_O(W) |W|^{-1}} (h_\epsilon * h_\epsilon)(r) + \gamma_2(f) (\mathbb{E} \left[\hat{g}_O(r) \right] - 1) + \gamma_2^O(f, W) \quad (C.39)$$

where

$$\eta(W) = \frac{\Lambda_Z(W)}{\Lambda_O(W)} \quad (C.40)$$

$$\gamma_2^O(f, W) = \eta(W)^2 \gamma_2(f) + (1 - \eta(W))^2 \gamma_2^E(f) + 2\eta(W)(1 - \eta(W)) \gamma_2^{EZ}(f) \quad (C.41)$$

Thus, whether X is motion-invariant or not, the mean of the involved summary statistics take approximately the same shape, and the estimation procedures can be carried out in the same way regardless. Of course, for pathological cases with all points lining the ROI edge, the above approximations can be bad, but this is a general problem and not unique to the methods presented here. Such cases can be avoided in practice, as the ROI can be chosen freely within the cell to obtain a favorable situation with relatively few points near edges.

Appendix D Selection of R and U

The sets R and U must be chosen in a way that reflects the size of blinking clusters, both in time and space. Since we are interested in the weights on the blinking-cluster term $(h_\epsilon * h_\epsilon)(r)$, we should pick R to reflect where this term is informative (different from 0), and explore this region well. Similarly for U , we need to explore the informative range of values where the CDF $\gamma_1(P_u)$ moves between 0 and 1.

As $(h_\epsilon * h_\epsilon)(r)$ can be estimated using only the observed localization uncertainties, it is straightforward to find a range of r -values where $(h_\epsilon * h_\epsilon)(r)$ exceeds some small threshold, say $(h_\epsilon * h_\epsilon)(r) > 0.001$. In addition, since standard kernel estimators of the mark and pair correlation functions can have considerable bias (and variance) for small values of R , it is advisable to exclude small values of r . The values of r that should be excluded depends primarily on the kernel bandwidth and the observed pairwise point distances. For all fitting in this article, we have chosen R as an evenly spaced grid between twice the kernel bandwidth and the first time $(\widehat{h_\epsilon * h_\epsilon})(r)$ dips under 0.001, with a step size of the smallest observed nearest-neighbor distance in the dataset.

For U we are at a slight disadvantage, as we do not apriori know where $\gamma_1(P_u)$ takes informative values. Thus, we propose the following iterative method for determining U : first, pick \tilde{U} as a wide-spanning grid of u values, within which interval we can say with a large degree of certainty most of the fluorophores have bleached. Typically, this would be measured on a time-scale of a minute or two at most, but more qualified guesses can be obtained by simply plotting the arrival times in the dataset. Using \tilde{U} , we fit the PALM-IBCp model to data, and obtain rate estimates. If \tilde{U} was chosen poorly, the estimates will be of lower quality, but will still provide information about the timescale of blinking. Thus, using the estimated $\hat{\gamma}_1(P_u)$ on the basis of \tilde{U} , we pick a new U as an evenly spaced grid between 0 and the first u such that $\hat{\gamma}_1(P_u) > 0.99$, and the model is fit a final time with this U . For simulations and analysis of the LAT-data, we chose the initial \tilde{U} as an evenly spaced grid between 0 and 1 minute, with 30 gridpoints. The final U was then picked as suggested above, with U having 50 gridpoints.

References

Andersen, I. T., Hahn, U., Arnspang, E. C., Nejsum, L. N. & Jensen, E. B. V. (2018), 'Double Cox cluster processes — with applications to photoactivated localization microscopy', *Spatial Statistics* **27**, 58–73.

Annibale, P., Vanni, S., Scarselli, M., Rothlisberger, U. & Radenovic, A. (2011a), 'Identification of clustering artifacts in photoactivated localization microscopy', *Nature methods* **8**(7), 527.

Annibale, P., Vanni, S., Scarselli, M., Rothlisberger, U. & Radenovic, A. (2011b), 'Quantitative photo activated localization microscopy: unraveling the effects of photoblinking', *PloS one* **6**(7), e22678.

Baddeley, A., Rubak, E. & Turner, R. (2015), *Spatial Point Patterns*, Apple Academic Press Inc.

Betzig, E., Patterson, G. H., Sougrat, R., Lindwasser, O. W., Olenych, S., Bonifacino, J. S., Davidson, M. W., Lippincott-Schwartz, J. & Hess, H. F. (2006), 'Imaging intracellular fluorescent proteins at nanometer resolution', *Science* **313**(5793), 1642–1645.

Coltharp, C., Kessler, R. P. & Xiao, J. (2012), 'Accurate construction of photoactivated localization microscopy (palm) images for quantitative measurements', *PLoS One* **7**(12), e51725.

Daley, D. J. & Vere-Jones, D. (2007), *An introduction to the theory of point processes: volume II: general theory and structure*, Springer Science & Business Media.

Davies, R. B. (1973), 'Numerical inversion of a characteristic function', *Biometrika* **60**(2), 415–417.

Deschout, H., Zanacchi, F. C., Mlodzianoski, M., Diaspro, A., Bewersdorf, J., Hess, S. T. & Braeckmans, K. (2014), 'Precisely and accurately localizing single emitters in fluorescence microscopy', *Nature methods* **11**(3), 253.

Fricke, F., Beaudouin, J., Eils, R. & Heilemann, M. (2015), 'One, two or three? probing the stoichiometry of membrane proteins by single-molecule localization microscopy', *Scientific reports* **5**, 14072.

Gelfand, A. E., Diggle, P., Guttorp, P. & Fuentes, M. (2010), *Handbook of spatial statistics*, CRC press.

Griffié, J., Pham, T., Sieben, C., Lang, R., Cevher, V., Holden, S., Unser, M., Manley, S. & Sage, D. (2020), 'Virtual-SMLM, a virtual environment for real-time interactive SMLM acquisition'.

Hummer, G., Fricke, F. & Heilemann, M. (2016), 'Model-independent counting of molecules in single-molecule localization microscopy', *Molecular biology of the cell* **27**(22), 3637–3644.

Karathanasis, C., Fricke, F., Hummer, G. & Heilemann, M. (2017), 'Molecule counts in localization microscopy with organic fluorophores', *ChemPhysChem* **18**(8), 942–948.

Lin, Y., Long, J. J., Huang, F., Duim, W. C., Kirschbaum, S., Zhang, Y., Schroeder, L. K., Rebane, A. A., Velasco, M. G. M., Virrueta, A. et al. (2015), 'Quantifying and optimizing single-molecule switching nanoscopy at high speeds', *PloS one* **10**(5), e0128135.

Ober, R. J., Tahmasbi, A., Ram, S., Lin, Z. & Ward, E. S. (2015), 'Quantitative aspects of single-molecule microscopy: Information-theoretic analysis of single-molecule data', *IEEE Signal Processing Magazine* **32**(1), 58–69.

Ovesný, M., Křížek, P., Borkovec, J., Švindrych, Z. & Hagen, G. M. (2014), 'Thunderstorm: a comprehensive imagej plug-in for palm and storm data analysis and super-resolution imaging', *Bioinformatics* **30**(16), 2389–2390.

Patel, L., Gustafsson, N., Lin, Y., Ober, R., Henriques, R., Cohen, E. et al. (2019), 'A hidden markov model approach to characterizing the photo-switching behavior of fluorophores', *The Annals of Applied Statistics* **13**(3), 1397–1429.

Rollins, G. C., Shin, J. Y., Bustamante, C. & Pressé, S. (2015), 'Stochastic approach to the molecular counting problem in superresolution microscopy', *Proceedings of the National Academy of Sciences* **112**(2), E110–E118.

Sengupta, P., Jovanovic-Talisman, T., Skoko, D., Renz, M., Veatch, S. L. & Lippincott-Schwartz, J. (2011), 'Probing protein heterogeneity in the plasma membrane using palm and pair correlation analysis', *Nature methods* **8**(11), 969.

Shivanandan, A., Deschout, H., Scarselli, M. & Radenovic, A. (2014), 'Challenges in quantitative single molecule localization microscopy', *FEBS letters* **588**(19), 3595–3602.

Shtengel, G., Galbraith, J. A., Galbraith, C. G., Lippincott-Schwartz, J., Gillette, J. M., Manley, S., Sougrat, R., Watterman, C. M., Kanchanawong, P., Davidson, M. W., Fetter, R. D. & Hess, H. F. (2009), 'Interferometric fluorescent super-resolution microscopy resolves 3d cellular ultrastructure', *Proceedings of the National Academy of Sciences* **106**(9), 3125–3130.

Small, A. & Stahlheber, S. (2014), 'Fluorophore localization algorithms for super-resolution microscopy', *Nature methods* **11**(3), 267.

Staudt, T., Aspelmeier, T., Laitenberger, O., Geisler, C., Egner, A., Munk, A. et al. (2020), 'Statistical molecule counting in super-resolution fluorescence microscopy: Towards quantitative nanoscopy', *Statistical Science* **35**(1), 92–111.

Stoyan, D. (1984), ‘On correlations of marked point processes’, *Mathematische Nachrichten* **116**(1), 197–207.

Yamanaka, M., Smith, N. I. & Fujita, K. (2014), ‘Introduction to super-resolution microscopy’, *Microscopy* **63**(3), 177–192.

Zhang, B., Zerubia, J. & Olivo-Marin, J.-C. (2007), ‘Gaussian approximations of fluorescence microscope point-spread function models’, *Applied optics* **46**(10), 1819–1829.